Available online at www.sciencedirect.com

ScienceDirect

Journal of Magnesium and Alloys 6 (2018) 23–43

www.elsevier.com/locate/jma

Review

Review of magnesium-based biomaterials and their applications

Nurettin Sezer[a], Zafer Evis[b,*], Said Murat Kayhan[b], Aydin Tahmasebifar[b], Muammer Koç[a]

[a] *Sustainable Development Divison, Hamad Bin Khalifa University, Qatar Foundation, Education City, Doha, Qatar*
[b] *Engineering Sciences, Middle East Technical University, PO Box 06800, Ankara, Turkey*

Received 15 June 2017; received in revised form 25 February 2018; accepted 27 February 2018
Available online 16 April 2018

Abstract

In biomedical applications, the conventionally used metallic materials, including stainless steel, Co-based alloys and Ti alloys, often times exhibit unsatisfactory results such as stress shielding and metal ion releases. Secondary surgical operation(s) usually become inevitable to prevent long term exposure of body with the toxic implant contents. The metallic biomaterials are being revolutionized with the development of biodegradable materials including several metals, alloys, and metallic glasses. As such, the nature of metallic biomaterials are transformed from the bioinert to bioactive and multi-biofunctional (anti-bacterial, anti-proliferation, anti-cancer, etc.). Magnesium-based biomaterials are candidates to be used as new generation biodegradable metals. Magnesium (Mg) can dissolve in body fluid that means the implanted Mg can degrade during healing process, and if the degradation is controlled it would leave no debris after the completion of healing. Hence, the need for secondary surgical operation(s) for the implant removal could be eliminated. Besides its biocompatibility, the inherent mechanical properties of Mg are very similar to those of human bone. Researchers have been working on synthesis and characterization of Mg-based biomaterials with a variety of composition in order to control the degradation rate of Mg since uncontrolled degradation could result in loss of mechanical integrity, metal contamination in the body and intolerable hydrogen evolution by tissue. It was observed that the applied methods of synthesis and the choice of components affect the characteristics and performance of the Mg-based biomaterials. Researchers have synthesized many Mg-based materials through several synthesis routes and investigated their mechanical properties, biocompatibility and degradation behavior through in vitro, in vivo and in silico studies. This paper is a comprehensive review that compiles, analyses and critically discusses the recent literature on the important aspects of Mg-based biomaterials.

Keywords: Mg-based biomaterials; Mechanical properties; Implant; Biomedical applications; Biodegradation.

Contents

* Corresponding author.
E-mail address: evis@metu.edu.tr (Z. Evis).

https://doi.org/10.1016/j.jma.2018.02.003

1. Introduction

From materials science point of view, biomaterials can be classified into four different groups as metals, ceramics, polymers and composites. Among these groups, ceramics such as calcium phosphates are widely used as a coating material since they exhibit non-toxicity, good biocompatibility and osteoconductivity [1]. However, they possess poor mechanical properties and high corrosion rate in acidic environment, which restrict their usage as bone implant in load bearing areas [1].

Polymeric biomaterials are widely used for bone tissue engineering applications since they are formable into complex shapes, and their surface properties can be easily modified. Additionally, chemical and mechanical properties of polymers can be altered to certain degrees during sterilization. However, application of polymers is limited due to their unsatisfactory mechanical properties. Moreover, some toxic additives such as plasticizers, antioxidizers or stabilizers used in synthesis of polymers can be harmful to the host tissue causing leaching in body fluid [2].

Metal implants are usually preferred to repair bone fracture owing to their outstanding mechanical properties [3]. Stainless steel-, Co- and Ti-based alloys are well-known examples for the commercially available bone implants. Metals are favored for long-term, durable and load bearing implants since they exhibit high strength and outstanding ductility that lead to high resistance to fracture [3]. In addition, metal implants with complex architecture can be produced through various available production methods such as casting, machining and powder metallurgy (PM) [3]. Their biocompatibility and matching mechanical properties to bone are two important factors for implants [3]. Biocompatibility of metallic implants is affected by corrosion and wear. In metallic implants, harmful metal ions arising from corrosion and wear may lead to inflammation, cell apoptosis and other destructive tissue reactions [3,4]. It was reported that release of Cr (Co–Cr alloys), Nb, V and Ni (Ti-based) ions may cause detrimental tissue reaction by exceeding the concentration limit of these elements in tissue or body fluid [3,4]. Ni, as an example, is a highly cytotoxic, genotoxic, carcinogenic and mutagenic element.

Mg and its alloys differ from other biomaterials by presenting compatible mechanical and physical properties to human bone. Their densities and elastic modulus are fairly close to each other which remove elastic mismatches between implants and the bone [5,6]. Moreover, Mg is naturally present in bone composition, and it is one of the required metals for the metabolism [7]. However, the fundamental problem of Mg-based implants is their low corrosion resistance resulting undesirably fast and unexpected degradation within a living system. Research investigations have been aimed to enhance the corrosion resistance and to offer industrially applicable Mg-based biodegradable implants. Furthermore, it is projected that Mg-based biodegradable implant will shift the direction of medical sector in near future as their commercial products start to appear in the market.

Implant material is desired to have very similar mechanical properties with the bone. However, in the current practice, most of the metals used in biomedical applications exhibit significantly higher mechanical properties than the bone. This causes well-known phenomenon of stress shielding, the results of which are bone-matter decomposition and loss of its strength. Stress shielding occurs when the implant carries higher proportion of the applied load, so the adjacent bone is exposed to a reduced load and loses its density in response [8,9]. Among various metal implants, Mg alloys stand out to have Young's modulus most similar to cortical bone (Mg: 40–45 GPa, Cortical bone: 10–27 GPa) whereas the Young's modulus of Ti-based and 316L stainless steel are 110 and 193 GPa, respectively [8,9].

Biodegradable metal implants are new generation of metal implants that exhibit improved corrosion resistance in body fluid during healing process of host tissue [10]. The main duty is to support the host tissue with a slow corrosion rate in the body fluid, and then dissolve completely after healing of the host tissue with no implant debris [10,11]. Among biodegradable metal implants, Mg, Fe and Zn, which are also known as smart implants, have been widely investigated in recent years. The most significant challenge with such biodegradable implants is to maintain their mechanical integrity during healing period of the host tissue [12]. Mg- and Fe-based implants exhibit good mechanical properties as hard tissue implants. However, high corrosion rate of Mg-based materials and very

low corrosion rate of Fe-based materials limit their application as biodegradable implants. Thus, degradation rate of pure Mg should be improved via alloying and surface engineering to use as biodegradable metal implants [12,13].

This study aims to present a comprehensive and critical review of recent research and technological advances on Mg-based biomedical implants. The following section briefly summarizes the most recent Mg-based biomedical implant products to give readers clear idea about where industry and commercialization fronts have been heading in this field. The third section focuses on synthesis and fabrication of Mg-based biomedical implants. Section four is more on characteristics of Mg-based biomedical implants presenting microstructural, surface, mechanical, biological and degradation characteristics of various Mg alloys. Fifth section provides a summary about computational aspects of Mg-based biomedical implants from fabrication and degradation points. Section six discusses potentials for Mg-based composites including Mg-ceramics and Mg-polymers composites. Final section provides a summary of this paper along with critical and comparative discussions ending with a list of recommendations for future studies.

2. Magnesium (Mg)-based biomedical implants and recent applications

The commercially available Mg-based biodegradable implants have been new in the market dating back to 2010s. Magnezix® (brand name of Mg-based implant in the market) is the first approved and CE-certified biodegradable screw that has been manufactured using PM route [14]. It has been approved for bone fixation and fragments [15]. It has more appropriate mechanical properties than commercially available Ti. For instance, owing to its close elastic modulus to natural bone, it hinders stress shielding that could even cause implant loosening. Moreover, it is free of Aluminum (Al), therefore, it is less likely to show any allergenic or toxic side effect [15]. Magnezix® has a yield strength (YS) greater than 260 MPa, a ultimate tensile strength (UTS) greater than 290 MPa and an elastic modulus about 45 GPa. It has an ability to elongate as high as 8%. After material and product design study started in 2009 for Magnezix®, preclinical studies were conducted between the years 2010 and 2012 [14]. The Magnezix® was approved by CE certification for 30 days in May 2013. It was put first in EU market and then the rest of the world. It has been reported that more than 4000 Magnezix® screws were sold around the world since then. The company continued to expand their product range with different screw sizes.

Commercially available Mg-based implants have been compared with other biodegradable and non-Mg implants. They have been tried by in vivo studies as well. They have been implanted in 33 mini-pigs and 20 humans [16]. No toxicity or allergenic reactions were observed. They preserved mechanical integrity themfor six months that could be regarded as long-term for fixation implants. After that, three generations of absorbable metal stents have successfully been implanted into animals and humans [16]. Schmidt et al. compared three biodegradable stents namely: The Absorb GT1™ (Abbott Vascular, Temecula, CA), DESolve® (Elixir Medical Corporation, Sunnyvale, CA) and the Magmaris® (BIOTRONIK AG, Bülach, Switzerland). The Absorb GT1™ and DESolve® are made of polymers whereas Magmaris® is an Mg-based PLLA coated stent. They were successfully approved in clinical trials [17]. According to the tests, Magmaris® expanded quickly and it was more stable in terms of mechanical performance. Although all the stents had sufficient radial strength, metallic one had the highest. Windhagen et al. conducted a comparison study between Magnezix® and Ti screws in 26 patients to assess their difference regarding patience comfort and biological effect during an implantation period of six months. It was reported that there was no statistically significant difference between two types of screws in terms of human comfort and poor biological reaction. All patients were satisfied with the Magnezix® except one patient who had suffered from long-last wound problem [18]. It showed that there was no distinct difference in terms of functionality but second surgical operation for implant removal was abolished for Mg based material.

3. Fabrication of Mg-based implants

This section presents the synthesis of Mg alloys and fabrication of implants based on these alloys. Ball milling in PM encompasses mechanical alloying of two or more alloy powders with hardened steel balls for extended periods of time. This process consists of welding, fracturing and rewelding resulting in fine microstructure, small grain size and alloying of the powder particles [19]. There are many factors that influence the characteristics of the end-product powders including ball-to-powder ratio, milling time, turning speed, preventive atmosphere and temperature.

The effect of milling time (15, 30 and 37.5 h) on the mixture of Mg and Fe powders was investigated [19]. The ball-to-powder ratio and rotation speed were kept the same as 10:1 and 350 rpm, respectively. More than 37.5 h ball milling caused to decrease in peak height in the XRD referring that longer milling time decreases crystallinity of the alloyed powder. Additionally, grain size continuously decreased to the size of 13–30 nm by increasing milling time. Chaubey et al. also investigated the effect of milling time on grain size and shape at room temperature (RT) for 100 h. It was reported that an heterogeneous microstructure including two types of clustering (Mg and Mg–Al areas) was observed. The average particle size was 600 μm due to cold welding until 20 h of milling whereas sizes of Mg (< 450 μm) and Al (< 44 μm) powders were smaller than the 20 h alloy. The average particle size decreased to 70 μm after milling for 40 h due to fracturing [20]. During the cold welding stage, grain size was even higher than the sizes of starting powder. However, the grain size started to decrease with start of fracture process of ball milling.

Ball milling is not used to alloy only the metals but ceramics as well. Mg and hydroxyapatite (HAp) mixtures were synthesized through ball milling for 4 h under protective argon atmosphere [21]. The optical images of ball-milled mixture

showed a uniform Ca and P distribution in the microstructure. It was a successful study since it uniformly distributed Ca and P that suppresses corrosion. Non-uniform distribution could lead localized corrosive attack on the end-product.

An effort has been put forward to overcome enormous cold welding in milling by using lubricant agents. It is especially vital for materials which are ductile and with low melting temperature. Feng et al. used stearic acid (5%) in order to limit cold welding in ball milling of Mg, Al and Zn for 20 h with 30:1 ball-to-powder ratio [22]. After ball milling, MgO was homogenously distributed with nano-level particle size. It showed that ball milling could improve microstructural characteristics and consequently mechanical properties of Mg–Al–Zn alloy.

Speaking of magnesium, ball milling could be hazardous due to its explosive nature [23]. Because of that, Mg was mixed with other metal elements in the absence of the hardened balls. An alternative solution was proposed to circumvent the high flammability of Mg [23]. Mg, Al and Zn powders were mixed for 1 h at 2500 rpm in a wet atmosphere to reduce the heat generation. The manufactured alloy without the balls was successfully subjected to extrusion that shows reliability of this method. Moreover, Yang et al. also mixed Mg, Al and $CaCO_3$ for 72 h to produce Mg alloy foam [24]. They manufactured a well-structured porous Mg alloy. Due to low ignition of Mg, it was also a safer way than ball milling. Kang et al. obtained a mixture of Mg and NaCl as space holder to use in PM [25]. This mixture was exposed to spark plasma sintering (SPS) successfully under an applied pressure of 20 MPa. The space holder was used to create pores as well as to prevent excessive cold-welding.

In Mg-based alloy studies for biomedical implants, investigators tend to purchase Mg and its alloy powders. However, Mg–Zn–Al alloy powders were manufactured by argon atomization and sieved to obtain particles smaller than 150 μm [26]. The atomization results in spherical grain that offers uniform microstructure. The alloy is then powder processed successfully. Manufacturing porous Mg implants with spherical powders offers samples with more predictable material properties. Zhou et al. also used rapid solidification to manufacture Mg–Zn and Mg–Zn–Ca [27]. Powders were produced by melting of constituent powders and rapidly cooling by splat quenching under noble gas atmosphere.

PM offers to produce biodegradable Mg implants that can have controlled interconnected porous structure for enhanced biological interaction with the environment of the host tissue or bone. However, the degree of porosity is critical for corrosion type (aggressive localized attacks such as pitting or galvanic corrosion) and rate (mm/year) [28]. Due to negative effect of pores that weaken materials mechanically and electrochemically, it is important to optimize porosity level as well as the distribution and shape of the pores. Therefore, PM studies have been intensively focused on production of controlled or designed porous biodegradable implants [29–32].

The virtue of PM over other biodegradable implant manufacturing methods including extrusion and casting was investigated [33]. The PMed WZ21 alloy had finer and more homogenous microstructure than other two methods. It was also detected that there is more secondary phase formation in the extruded and as-cast alloys. Compatible with these findings, the extruded and as-cast alloys had lower corrosion resistance than the powder-processed alloy due to higher secondary phase formation that acts as a kind of galvanic cell. Although, YS and UTS of as-cast and extruded alloys did not differ from each other, PMed alloy had a YS of 292 MPa and an UTS of 346 MPa due to its fine and homogenous microstructure. It could be said that PM improved WZ21 alloy not only mechanically but also electrochemically. It was also investigated how secondary phase (MgO) affects microstructural chracteristics of Mg in the presence of HAp. Compatible with the study of Cabeza et al., the addition of MgO decreased the corrosion resistance and compressive strength [34]. Beyond that, Mg-HAp without MgO exhibited the best mechanical integrity. MgO acts as a galvanic cell in the microstructure that accelerates degradation. Accordingly, the corrosion resistance of the Mg-HAp with MgO diminished. It can be deduced that secondary phase existence in the microstructure could worsen the mechanical and electrochemical properties.

In a different study, porous Mg–Zn alloy was manufactured by PM route under an applied pressure of 100 MPa and heat treatment temperature of 500–580 °C. It was found that there was an inverse correlation among porosity and compression strength and elastic modulus [30]. The highest compression strength and elastic modulus were observed at 550 °C so it was chosen as the optimum heat treatment temperature. Tahmasebifar et al. investigated the effect of compaction pressure, sintering temperature and surface conditions on relative density, bending strength, corrosion resistance and cell viability of powder-processed AZ91D through design of experiment (DOE) [35]. It was stated that increasing compaction pressure (150–250 MPa) improved the relative density and bending strength. On the other hand, sintering time did not significantly affect the material properties of AZ91D. It was also revealed that the micro-patterned/textured surface with open pores showed higher cell viability than the smooth surface. The study specifically showed that it was feasible to manufacture Mg alloy with open pores on the surface with a structure via PM. A similar study was carried out by Kayhan et al. by manufacturing highly porous Mg alloy at lower compaction pressures (25 and 40 MPa) [36]. The relative density and hardness decreased as compaction pressure increased. Increasing the sintering time (30–150 min) did not increase relative density but hardness due to the formation of intermetallic phase. A surface with one-way channels was designed with a specific aspect ratio (1.25) to increase cell viability. Aspect ratio is important not only for cell viability but also for cell attachments. The study showed that a surface with the channels of 200 μm width and 160 μm height was biocompatible and favorable for biomedical applications [36]. Bi et al. investigated the relation between ultimate compressive strength (UCS) and porosity of pure Mg manufactured by powder processing (compacted under 300 MPa, heat-treated 400 °C and then 550 °C for 2 h each). It was found that increasing porosity to 40% with space holder decreased the UCS from 170

to 25 MPa [29]. Xia et al. have also reported that the YS of AZ31 Mg alloy scaffolds decreased as porosity increased from 60% to 75% [37]. Pore size also affected energy absorption and consequently the UCS of the alloy. Pore sizes were 1.2, 1.5, 1.8 and 2.0 mm but 1.5 mm differed from others due to the ratio between specimen and pore sizes.

Organic and inorganic materials such as PMMA, ammonium hydrogen carbonate, PE-VA, PPco1PB, PP, $CaCO_3$ "so-called as space holder" were used to produce interconnected porous specimens [24,29,38,39]. A suitable space holder in terms of material properties is required to avoid its negative effect during manufacturing process. For instance, some space holder materials can react with matrix and affect negatively the porosity characteristics. Porosity and pore structure can be controlled by manipulating the content and particle shape of space holder. The more space holder content results in more interconnected porosity [39]. Similarly, it was reported that the sintered density is inversely proportional to the content of space holder (PMMA) as in pure Mg. Besides, PMMA had poor affinity to Mg [29]. Thus, it does not easily react with Mg. Yang et al. also used $CaCO_3$ to create pores in Mg-Al alloy foam with various concentrations of Al from 15 to 50 wt%. They emphasized that if the required conditions and processes, such as high pressure of compaction, at 620 °C of foaming temperature and 150 s of foaming time, are provided then the uniform pores can be obtained [24].

SPS has been used to create porous biodegradable implants from Mg alloy powders. It has been developed to prevent problems arising from sintering for longer times [40]. Due to its shorter time for sintering at relatively low temperature, oxidation or secondary phase formation were substantially hampered. Mg powders with the addition of Al_2O_3 (up to 5 vol%) and 60% NaCl as space holder were exposed to SPS while uniaxially-compacted under 20 MPa. Uniformly distributed 3D interconnected porous structure with average pore size of 240 μm and porosity of around 60% were observed in the microstructure. Moreover, no significant secondary phase formation or reaction among existing phases was observed in the XRD analysis referring that sintering was accomplished properly [41]. Sunil et al. carried out SPS on Mg/HAp powder mixture after 20 h ball milling to make more uniform distribution in the mixture [40]. The mixture sintered for 10 min under 50 MPa compaction pressure at 450 °C. Although secondary phase formation is not expected in SPS, MgO peaks were found at the XRD analysis. The researchers estimated that it was formed just after ball milling before sintering was not started. Moreover, it is expected that increasing the bioceramics (HAp in this case) amount increases hardness. On the contrary, Mg with the highest HAp addition had the lowest hardness that could be related to low sintering temperature of SPS. Sintering at low temperature could not be sufficient for proper bonding between Mg-HAp and HAp-HAp particles. Thus, sintering temperature and time should be carefully designed in SPS process in order not to suffer from mechanical performance. In another study, Mg-HAp mixture was exposed to SPS at 475 °C under 40 MPa pressure after 2 h ball milling with the purpose of enhancing corrosion resistance [42]. Similar to previous study, MgO peaks were observed in the XRD analysis in the presence of 20 wt% HAp. However, the researchers reported formation of MgO during the SPS process which is contrary to the results of Sunil et al. Xiong et al. succeeded to fabricate Mg/HAp composite with low porosity after 10 min sintering in microwave sintering furnace. In this method, a homogenous distribution of Mg and HAp particles was achieved. Furthermore, XRD results revealed that there was no incidence of any interaction between Mg and HAp during heat treatment [21].

Metal injection molding (MIM) is another PM method used in economical manufacturing of near net shape products. Some researchers have tried to manufacture Mg-based implants by MIM. Wolff et al. carried out a study on producing biodegradable implant from Mg–0.9Ca alloy powders through MIM method. The Mg alloy powders compacted under 100 MPa and heat-treated at 630–645 °C for up to 64 h under vacuum. An organic polymer binder was also used for stocking in the injection process. It was reported that a minimum of 8 h sintering time is required for necking between particles. It was also found that elastic modulus decreased as porosity increased. An interesting finding was about vacuum during sintering. Vacuum at elevated temperature, such as the sintering temperature, led to evaporate Mg alloy towards the internal surface of the furnace. Thus, vacuum is recommended for the first half an hour of sintering [39]. The manufacturing of porous biodegradable implants through cold isostatic pressing prior to the extrusion of Mg-HAp powder mixture is another research which is still being investigated [32]. Table 1 summarizes the results of available literature on porous Mg-based biodegradable materials.

Apart from metallic alloying elements, Mg was mixed with other elements or compounds to produce satisfactory biodegradable implant materials. For example, Mg was alloyed mechanically with nano-sized diamond powders, and then were cold-pressed-and-sintered under 1 GPa at 600 °C for 30 min [44]. The addition of nano-sized diamond particles into Mg powders increased corrosion resistance by creating a protective layer on the implant surface. However, the relative density decreased due to high hardness of nanodiamonds that do not easily deform. The undeformed diamond particles possibly caused more pore formation in the microstructure. They deduced that Mg with nano-sized diamond manufactured by PM is a suitable candidate for porous biomedical implant. Kowalski et al. also manufactured Mg–4Y–5.5Dy–0.5Zr alloy with HAp addition by powder processing [45]. Compaction under 600 MPa followed by sintering at 550 °C for 2 h caused formation of the secondary phase. HAp addition enabled to produce implant samples with average porosity of 48% and elastic modulus of 7.1 GPa. HAp also helped to the formation of protective F^- layer that inhibits corrosion rate [45]. Furthermore, bioactive glasses were coated to increase corrosion resistance and mechanical performance of PMed alloys. Yazdimamaghani et al. coated Mg alloy (compacted under 400 MPa and sintered at 175 °C and then 600 °C for 2 h) with PCL and a silica-based bioactive glass mixture. Additional to the contribution of coating to mechanical stability,

Table 1
Investigations on porous Mg-based implant through various PM methods.

Material	Info	Reference
Porous Mg/5 vol% Al_2O_3	SPS (585 °C for 2 h under uniaxial pressing of 20 MPa), app. 60% porosity app. 240 μm grain size.	[43]
Porous pure Mg scaffolds	0–40% porosity, increasing PMMA content from 0% to 30%, conventional PM (compacted under 300 MPa, heat-treated 400 °C and then 550 °C for 2 h)	[29]
Mg scaffolds with increasing PCL-BG addition	35–40% porosity, ammonium hydrogen carbonate as space holder, conventional PM (compacted under 400 MPa and sintered at 175 °C and then 600 °C for 2 h)	[38]
Suture anchor screws	Mg–0.9Ca screw (metallic one) by Metal injection molding (MIM)	[39]

the coated alloy was degraded less than the uncoated sample [38]. The mixture of ball-milled pure Mg with various amount of 45S5 bioactive glass from 5 to 15 wt% was developed and manufactured under PM conditions [46]. The ball-milled powders were pressed under 10–15 MPa and heat treated in a microwave furnace at 600 °C for less than 25 min. The addition of bioactive glass improved both hardness and corrosion resistance continuously. Less hydrogen evolution of Mg alloy with 15 wt% contribute the corrosion resistance. However, the highest flexural strength and UCS were statistically found in the alloy with 10 wt% bioactive glass addition. The authors commented that the result arouse from the redundant secondary phase formation related to the amount of bioactive glass and internal microcracks which were deeper and larger.

4. Characteristics of Mg alloys

4.1. Contents

Alloying is one of the methods in which different metals at varying concentrations can be added to improve the ductility, strength and corrosion properties of pure Mg. Improvements in strength and corrosion are primarily linked to modification of microstructural characteristics; particularly a reduction in grain size compared to pure Mg. The majority of research investigating Mg alloys has focused on improving all of these characteristics for commercial purposes. Hence, most of the research on biomedical Mg alloys are conducted with alloys that are originally developed for aerospace, defense and automotive industries [47].

Generally, Mg alloys contain aluminum (Al) or rare earth elements (REEs) [54]. Al is well-known as a neurotoxicant and its accumulation is associated to various neurological disorders as Alzheimer, dementia and senile dementia diseases. On the other hand, severe hepatotoxicity was noticed after the implementation of REEs such as praseodymium, cerium and yttrium. Thus, researchers recently concentrated on investigation of biologically safe Mg alloys, comprising non-toxic elements such as Ca, Zr, Zn and Mn. Other alloying components that are being investigated include Sr, Li, Sn, Si, Bi, Cd, and Ag. Alloys of Mg can be binary, ternary or more. The components and the composition of the alloys contribute to various mechanical properties as well as the corrosion behavior of Mg.

Alloying with Al enhances the corrosion resistance of Mg. AZ31, AZ61, and AZ91 are common Mg–Al–Zn alloys with moderate corrosion rates. Zn is one of the common alloying elements for Mg. Presence of 6% Zn in Mg alloy is reported to improve the corrosion resistance [55]. Ca is another well-known alloying element which accelerates the bone growth. Mechanical properties and corrosion behavior of Mg–Ca alloys can be adjusted by controlling the Ca content [54]. REEs are other common incorporating elements of Mg alloys. Addition of REEs into Mg–Al–Zn alloys is reported to further improve the corrosion resistance [28].

Incorporating Ca in Mg alloy can improve the corrosion resistance [56]. Li et al. fabricated binary Mg–Ca alloy at varying Ca contents from 1 to 20 wt% to investigate its biodegradability within bone. Alloys of high Ca content including Mg–5, 10 and 20Ca were found to be very brittle. The mechanical properties and biocorrosion behavior of Mg–Ca alloy are adjustable by controlling Ca content. The YS, UTS and elongation for as-cast Mg–Ca alloy samples decreased with increasing Ca content. Cytocompatibility evaluation results indicated that Mg–1Ca alloy induces no toxicity to cells. Both the in vitro and in vivo evaluations showed formation of a mixture of $Mg(OH)_2$ and HAp layer on the surface of Mg–1Ca alloy during immersion and implantation periods [54]. A similar study by Rad et al. suggested Mg–0.5Ca alloy as a promising candidate for biodegradable implants due to its high corrosion resistance [57].

Knowing that incorporating Ca reduces the degradation rate, Ca-containing Mg alloys have been investigated for their degradation behavior and mechanical integrity. Addition of Ca was noticed to improve the corrosion behavior of Mg alloys. Immersion test of AZ91Ca into modified simulated body fluid (SBF) showed only a marginal decrease in the UTS by 15% and elongation to fracture by 20% [58]. Addition of Zn was also reported to improve the corrosion resistance of Mg alloys. The in vivo degradation behavior of Mg–Al–Zn alloy implanted intramedullary into the femora of rabbits was investigated by Jingjing et al. After a nine-week period, microscopic evaluations showed formation of a thin layer of calcium phosphate around the implants. In vivo degradation rate of Al–Zn containing Mg alloys AZ31B was slower than the pure Mg [59]. Another zinc containing Mg alloy Mg–6Zn was investigated [55] and very similar results with the previous research of Huang et al. were obtained.

The mechanical and corrosive characteristics of the Mg-based alloy (MgNd2) were investigated by Seitz et al. The study suggested that Nd_2 can be used as an adequate alloying element for resorbable applications in low loaded tissue

[60]. A new Mg-based alloy (LANd442) containing 90 wt% Mg, 4 wt% Li, 4 wt% Al, and 2 wt% Nd was developed by Hampp et al. Biocompatibility of this alloy was investigated in a rabbit model for a duration of 26 weeks. In this period, a relatively slow degradation was observed with the LANd442 alloy. Formation of an additional bone at the implant's location as well as accumulation of small amount of subcutaneous gas was observed. The LANd442 Mg alloy lead to considerable non-inflammatory bone remodeling processes in which new growth of bone in the periosteal region predominated. For this reason, the study suggested that LANd442 appears to be a less suitable degradable implant material for cortical bone applications [61]. After this study, Hampp et al. investigated the earlier times of healing process since it could represent possible early incidence of bone remodeling phase. They investigated the biocompatibility of two Mg-based alloys LAE442 and LANd442 and compared them with titanium in the first 4 and 8 weeks of implantation. The study identified interesting changes in the bone structure in the very early stage of implantation of Mg alloys and Ti. The investigated Mg alloys also revealed a good clinical tolerance which allows for their assessment as suitable osteosynthetic materials. However, compared to the studies with longer implantation periods, this short-term biocompatibility cannot conclude on long term effects. Thus, it was suggested that for a complete conclusion, implant materials should be investigated for at least 6 months period of implantation [62].

Studies showed that Sr significantly improves the osteoblastic activity and bone formation in vivo [63]. Therefore, it was considered as one of the promising biocompatible alloying element in Mg alloys [64]. Li et al. [63] investigated the biodegradable Mg–Zr–Sr alloys in vitro and in vivo. The study revealed that the addition of more than 2% Sr in Mg–Zr–Sr alloys results in rough boundaries distributed by a secondary phase of Mg17Sr2. This phase may trigger galvanic effects in the Mg–Zr–Sr alloys, leading to accelerated corrosion of the Mg matrix. The study reported that addition of less than 2% Sr ensures a significantly reduced corrosion rate for Mg–Zr–Sr and Mg–Sr alloys. The combined effects of Sr and Al on corrosion behavior of Mg alloys were studied by Nam et al. [65] with various Sr contents. Addition of Sr to Mg–5Al alloy significantly influenced the grain boundaries, corrosion resistance and surface film. The precipitation of Mg–Sr and Al–Sr phases was inhibited by the formation of Mg17Al12 phase at the grain boundaries. In addition, Sr addition contributed to the formation of an $Al(OH)_3$ protective film on the surface. The study by Bornapour et al. [66] demonstrated that a Sr–HAp layer was formed on the surface of the binary Mg–Sr alloy after immersion in SBF. This surface layer also improved the corrosion resistance.

Addition of Ce improved the corrosion resistance of Mg alloys [66], such as Mg–Zn–Zr alloys [67] and Mg–Al–Zn alloys [68]. Mg12Ce and Mg17Ce2 phases precipitate and distribute along the grain boundaries which effectively decrease the grain size of Mg–Zn–Zr alloys. During solidification process of Mg–Al–Ce alloys, Ce particles aggregate at the solid–liquid interface which reduces the atomic diffusion rate inhibiting the growth of Mg matrix grains. During solidification, Al–Ce phases form and distribute along grain boundaries which prevent the sliding of the boundaries at the course of deformation. The Al–Ce particles also reported to have a pronounced effect on the corrosion rate of Mg–Al–Ce alloys. When the Ce content of the alloy is high, Al11Ce3 acicular particles reduce the corrosion rate of Mg alloys by forming a network on Mg matrix [69].

Most of the research studies reported promising results for the application of Mg alloys as implant material. Their desirable mechanical properties, biocompatibility, and biodegradability are attractive features to be selected for implants. It is believed that Mg and Mg alloys are a new generation of biomaterials and they will play an important role in revolutionizing orthopedic, cardiovascular and dental applications [70].

4.2. Microstructural characteristics

The microstructure, such as the grain size, grain boundary and phase distribution significantly affect the corrosion performance of Mg alloys. Grain refinements lead to changes in the density of grain boundaries and distribution, which alter the mechanical properties as well as the corrosion behavior of Mg alloys [69]. The alloying elements, applied metallurgical processes and process conditions have influence on the microstructure of Mg alloys [71–75].

Cheng et al. [71] investigated the corrosion performance of as-cast and as rolled Mg–6Bi–2Sn alloys. Compared to the as-cast alloy, significant grain refinement and uniform distribution of second phase particles were achieved after rolling. Therefore, as-rolled alloy exhibited a higher corrosion resistance than the as-cast one. The remarkably deceased corrosion rate of as-rolled Mg–6Bi–2Sn alloy is credited to refined grain size, finely dispersed particles of secondary phase, favorable crystal orientation and the formation of a passivity film on the surface.

Lu et al. [72] investigated the corrosion behavior of Mg–3Zn–0.3Ca alloy in SBF. Heat treatment was applied to modify grain size and secondary phase volume fraction and its effect on the corrosion behavior was then determined. The study revealed that fraction of secondary phases and grain size are the two key factors which control the corrosion rate. The sample with the smallest grain size but the largest fraction of secondary phase has the lowest corrosion resistance, because the secondary phase causes the galvanic corrosion which surpasses the favorable influence of fine grain size. Similarly, the sample with the lowest secondary phase fraction but the largest grain size also has a low corrosion resistance because the large grain size accelerates the corrosion rate. The minimum corrosion rate was reported with the alloy heat-treated at 420 °C for 24 h since it balanced the grain size and fraction of secondary phase.

Addition of Zr reduces the grain size of Mg which results in improved ductility, smoothened grain boundaries and enhanced corrosion resistance. The ability of 1 wt% Zr–Mg alloy to absorb high loads is better than that of pure Mg [73].

It was reported that Sr has a high Mg alloying efficiency and refines the grain size in Mg alloys [52]. Mg–Sr alloy composed of α-Mg as a main phase and $Mg_{17}Sr_2$ and the amount of intermetallic phase increase with increasing Sr content [76]. Additionally, Sr increases the compressive strength, improves biocompatibility and bone formation. However, Sr > 2% in Mg–Zr–Sr alloys leads to $Mg_{17}Sr_2$ phase precipitation in the grain boundary and this intermetallic phase decreases the corrosion resistance. Thus, the level of Sr should be less than 2%. Sr enhances the replication of preosteoblastic cells, and stimulates bone formation. In Mg–Si–Sr ternary alloys depend on different composition of alloys four intermetallic phase can be formed which are $Mg_{17}Sr_2$, MgSrSi, $MgSi_2Sr$ and Mg_2Si. It was proved that high amount of (more than 14 wt%) intermetallic phase has negative effect on corrosion resistance of Mg alloys. The most effective factor in Mg–Si–Sr ternary alloys degradation is $Mg_{17}Sr_2$ intermetallic phase amount [77].

Mg–Ca–Si alloys are suitable candidates as biomedical implants because Ca and Si are naturally present in human body, involved in crucial body functions and essential for the bone regeneration processes. Apart from their duties in the body, presence of Ca resulted in formation of intermetallic phase due to low solubility of Ca in Mg [78]. This intermetallic phase plays an important role in grain refinement when they are located in front of grain boundaries. The intermetallic phases of Mg–Ca–Si alloys are MgCaSi, Mg_2Si and Mg_2Ca and their presence depends on composition of alloy. It was proved that three different phase combination can be seen in Mg–Ca–Si ternary alloys. The phase can be predicted by considering the Ca/Si ratio. The phases for alloys of lower than 1.4 Ca/Si ratio are α-Mg + Mg_2Si + MgCaSi. If Ca/Si ratio is located between 1.4 and 1.7, the phases are α-Mg + MgCaSi and for Ca/Si higher than 1.7, they are α-Mg + Mg_2Ca + MgCaSi [79].

The main phases for the Mg–Zn alloys are α-Mg, $MgZn_2$, $MgZn_3$, Mg_7Zn_3 and MgZn. Previous studies showed that addition of Al into Mg–6Zn alloy resulted in formation of other intermetallic phases such as $Mg_{32}Al_{49}$, $Mg_{32}Zn_{49}$ and $Mg_{17}Al_{12}$, and formation of these phases are highly dependent on the amount of Al [80]. Addition of Al up to 3 wt% resulted in formation of eutectic phase while addition of Al more than 5 wt% changes morphology from eutectic to lamellar phase by formation of $Mg_{17}Al_{12}$ secondary phase. Thus, it can be concluded that Zn/Al ratio has significant role on the formation and morphology of phases [81].

Zhang et al. [74] investigated a biodegradable Mg–Nd–Zn–Zr (denoted as JDBM) alloy extruded at 320 °C at 8 and 25 extrusion ratios. The results show that the lower extrusion ratio leads to a better corrosion performance with finer grains and higher strength, but lower elongation. Their study at various extrusion temperatures revealed that the grain size increases with the increasing extrusion temperature due to the growth of recrystallized grain at a higher extrusion temperature [75].

4.3. Surface characteristics

Hierarchical structure of bone should be considered in bone implant designs [82,83]. For instance, human compact bone is a composite material with a hierarchical architecture from macro-scale to nano-scale. Human compact bone can be explained as follows. Osteons are fibers with 200 μm diameter that are composed of parallel lamellae and pores. The lamellae are built of fibers which are built from fibrils. Mineral HAp and collagen type I formed a composite at nano-scale. Thus, the wide range of scale should be taken into account to achieve a high grade of compatibility with host tissue [83].

There are important factors that should be considered to improve biocompatibility of implants such as corrosion rate, strength, wear resistance, flexibility and solubility in water [83]. Moreover, porosity, cavities or channels at micro scale play an important role in cell proliferation and ingrowth into the implant [83]. As explained, individual surface parameters such as roughness, chemical composition, electrical charge, wettability and crystallinity perform an important role in terms of compatibility [83]. The most important factor to attain a high degree of compatibility of an implant with host tissue is surface property of the implant. Also, surface properties have a significant effect on stress shielding, wear resistance and fatigue failure. Moreover, implant surface is a predominant factor on success or rejection of implanted material because it is in direct contact with the host tissue surface.

Surface roughness is a key factor for osseointegration rate and mechanical fixation of implant to bone [84]. It was proved that surface roughness at micro-scale range improves the new bone formation rate due to an increase in protein adsorption and cellular activity [84]. van Tol et al. showed that shear strength of bone-implant was increased by increasing surface roughness from 0.058 to 4.25 μm [85]. In another study, the bonding strength was increased (0.38–9.70 MPa) by increasing Ra (0.2–4 μm) values [86]. Ra values of Mg plates were measured between 5.66 and 6.44 μm. Previous studies showed that the optimum surface roughness improves the bone-implant bonding strength. Rønold et al. investigated the effect of surface roughness on bone-implant integrity. They showed that the best bone-implant integrity was achieved at Ra = 3.90 μm and there is a significant decline in bone-implant integrity by increasing Ra value from 5.07 to 11.03 μm [87]. In another study, there was a significant increase in bone cell activity by increasing surface roughness from 0.37 to 3.29 μm [88].

Pore size and pore morphology have a significant effect on cell attachment and proliferation. It was proved that pores with hexagonal morphology increase cell attachment more than the pores with spherical shape. Also, in vivo studies showed that the risk of infection decreases by increasing pore size after implantation (0.1 mm). On the other hand, increasing pore size negatively affected the mechanical properties of implants. Implants show brittle behavior when the pore size was increased from 100–200 to 350–450 μm. Thus, increasing the pore size declines elastic modulus, shear and compaction strength [89].

Combination of random macro, micro and nano-scale roughness on implant surface improves the integrity between implant and host tissue. Roughness on surface of an implant increases the protein accumulation and as a result improves cell attachment [90]. Thus, mimicking the bone surface with micro and nano-texture may promote osteointegration due to increase in mineral deposition [91]. Prodanov et al. manufactured three different pattern surfaces (150, 300 and 1000 nm). In vitro results proved that the best mechanical integrity was achieved on the surface with 300 nm roughness [90].

Branemark et al. modified the implant surface by using laser technology. It was reported that the rate of new bone formation at contact region increases due to bone bonding at nano-level. Also, pore size has a significant effect on in vivo behavior of implant. Shear stress was increased by increasing pore size from 100 to 200 μm while by increasing pore size from 200 to 300 μm, it was declined [92].

The optimum surface roughness should be found to increase cell attachment but it is not predominant factor in cell integration. The optimum size for roughness may depend on actual size of cell used in vitro studies. Mirhosseini et al. investigated the effect of laser patterning on cell attachment for Ti6Al4V implant. The patterned surfaces improve 2T3 osteoblast cell growth and uniform cell attachment. While, smooth surface cells accumulate on the implants in region which is near to the center of seeding [93].

4.4. Mechanical properties

It is vital to have sufficient and appropriate mechanical properties for biomedical implants during their life cycle. Durability in the implanted structure is a top priority issue for patient safety because the role of an implant is to support physically the damaged tissue during healing process. Moreover, biodegradable implants that have the highest mechanical properties do not necessarily mean that they will represent the best performance. For instance, an enormous difference between elastic moduli of implant and damaged bone may lead elastic mismatches and cause stress shielding especially in metallic biomaterials that are used for orthopedic applications. There are many ways to boost mechanical performance of biodegradable implants. At least but not less, two main routes can be named in order to enhance mechanical properties of Mg alloys that are alloying and combined manufacturing methods.

From mechanical point of view, Mg-based alloys have faced two challenges which are stress shielding for bone implants and “ductility and bendability” limitation for cardiovascular stent applications [94].

In many studies, researchers have tried to improve mechanical properties of Mg by alloying it with various elements such as Ca, Al, Zn, Zr and REEs. Mg has ability to create solid solution with many elements including Al, Zn, Ca and Sr due to its atomic size (about 320 nm) and hexagonal close-packed system [15]. The amount of alloying element was also tuned up to obtain the best mechanical performance as a biomedical implant [27,95–101]. Wang et al. reported that Y (2.5 wt% to 7.5 wt%) and Nd (1–4.2 wt%) content in extruded WE alloy caused a decrease in ductility while an increase in strength [95]. Hence, it can be said that their alloy is more appropriate for orthopedic implants than cardiovascular applications due to its low ductility. Homayun and Afshar investigated the effect of Al addition on the mechanical properties of as-cast Mg–4Zn–0.2Ca alloy. Though Al and Zn increase YS and UTS by solid solution and grain refinement strengthening, more than 3 wt% Al addition caused secondary phase ($Al_{12}Mg_{17}$) formation at grain boundaries and reduced elongation and UTS [97]. However, compressive strength was not affected as same as UTS by increasing amount of Al. The authors explained that tensile and compression stresses have different crack mechanism. The compressive strength increased due to the formation of secondary phase. Similarly, the Mg–Al binary alloy foam with 2% Al could withstand higher stress in compression test than the binary alloy with higher Al addition. It was related to the abundant secondary phase formation between Mg and Al that reduced mechanical integrity [24]. Compatible with previous study, Zhou et al. manipulated Nd content in the extruded Mg–1Mn–2Zn to make microstructure finer and to increase UTS and ductility. Increase in Nd content increased UTS and elongation; however decreased compressive strength since the Mg_7Zn_3 affected uniformity in the microstructure [27]. The effect of Mn addition to as-cast and heat-treated Mg–2Zn–0.5Ca alloy was also investigated by Yandong et al. Mn addition has a peak value of 1 wt% for the highest UTS and elongation [98]. They also reported that addition of Mn higher than 1 wt% caused the formation of brittle Mg–Zn intermetallic phase and reduced UTS and ductility. Shi et al. tried to optimize mechanical properties of Mg–Gd–Ca–Zr alloy by manipulating Ca addition up to 1.2 wt% [101]. Ca addition increased YS as well as compressive strength but decreased the ductility. They stated that Ca and Zr are good at grain refinement and helped to increase mechanical performance of the alloy for orthopedic applications. Yan et al. reported that YS and UTS had their highest values as Zn addition reached to 14.5 wt% due to uniform dispersion of Mg–Zn intermetallic phase in the microstructure. It was found that the extruded Mg–Zn binary alloy with Zn addition more than 14.5 wt% caused formation of coarser and strike-like grains that decreased the YS and UTS. However, elongation was affected from the increase in Mn addition differently. Addition of more than 14.5 wt% Mn continuously increased the ductility that made the alloy suitable for stent applications [100].

Mn was added to Mg–3Sn alloy to increase mechanical performance by the formation of intermetallic phases for stent applications [94]. Zhen et al. found that Mg–3Sn–0.5Mn alloy (23%) was more ductile than WE43 and AZ31 Mg alloys (12–21%) while their UTSs were at the same levels [102]. Intermetallic Mg_2Sn phase helped to improve mechanical performance of the alloy due to the fact that Sn is an effective strengthening element because of intermetallic phase. It can be concluded from previous studies that basic mechanisms in alloying that improves mechanical performance are solid

solution, precipitation hardening and grain refinement strengthening [15].

Increasing simultaneously the concentration of Sr and Ca decreased the mechanical properties due to secondary brittle Mg phase formation of those elements in Mg–Si–Sr–Ca alloy [103]. As in previous studies, secondary phase formation without a uniform distribution in the microstructures led to weaken the mechanical performance including UTS, YS and elongation. Brittle secondary formation that causes the lack of uniformity helped crack initiation.

Solution and aging treatments are two heat treatment processes to adjust mechanical properties in biomedical applications. Solution treatment increases ductility as it decreases strength. However, aging treatment causes a total opposite. Therefore, aging treatment could be suitable for bone implants whilst solution treatment or solution treatment followed by aging treatment for cardiovascular stent applications [104]. A study supported that aging treatment to the extruded Mg–3Nd–0.2Zn–0.4Zr alloy increased UTS. However, elongation remained as high as 26% without aging treatment [75]. Extrusion is regarded as more preferable manufacturing method for Mg alloys than casting due to its work hardening occurrence and solid solution strengthening mechanism inducing in the microstructure [27,105]. It was shown in multiple studies by comparing powder extrusion with other manufacturing methods. For instance, Sun et al. compared mechanical properties of the as-cast and extruded Mg–4.0Zn–0.2Ca alloy. The extruded ternary Mg alloy showed better mechanical properties due to the formation of secondary phases of Ca and solution hardening effect of Zn [106]. Wu et al. conducted a comprehensive comparison between as-cast, extruded and cyclic extrusion compressed (CECed) Mg–Zn–Y–Nd alloy for cardiovascular stent applications. The hot extruded Mg alloy exhibited higher YS and UTS. However, the CECed Mg alloy showed 1 and 2 times higher ductility. The authors explained higher ductility, lower YS and UTS with smaller grain size (about 1 μm), precipitation of secondary phases at grain boundaries and dislocation density by the cyclic plastic deformation in the microstructure [107]. The effect of three manufacturing methods (CEC, ECAP and hot extrusion) for cardiovascular applications on the tensile properties and ductility has been analyzed [108]. Contrary to Wu et al., the CECed alloy had the highest UTS and YS. The formation of intermetallic phase of Mg–Nd in the CECed alloy increased the tensile properties due to grain refinement and precipitation strengthening. However, it was noted that the ECAPed alloy had large grains than CECed alloy's in spite of the fact that their UTSs are close to each. Thus, the authors concluded that UTS is not only affected by grain size but also by dislocation density [108].

Fan et al. emphasized the positive effect of hot extrusion on mechanical properties of Mg–1.5Y–1.2Zn–0.44Zr alloy due to LPS structure of secondary phase ($Mg_{12}ZnY$). Similar to previous study, the hot extruded alloy had superior strength and ductility than as-cast and heat-treated alloys due to the grain size refinement effect and uniform secondary phase distribution [109]. Similarly, it was reported that ECAPed Mg–2Zn–Ca alloy containing 1 wt% β-TCP (789 HV) had higher hardness than as-cast alloy (539 HV) [110]. Accordingly, Gui et al. also reported the hot extruded Mg–Gd–Zn–Zr–Mn alloy had about 1 time more YS and UTSs [105]. It was also more ductile (18 to 21.3%) than as-cast and heat-treated counterparts. Zhang et al. also emphasized that ECAP increased UTS (161–267 MPa) and YS (85 to 217 MPa) of Mg–Gd–Nd–Zn–Zr alloy as well as the hardness due to the fact that ECAP helped formation of β_1 phase which hinders dislocation movements [111]. Mechanical properties of Mg-based biodegradable implants are compiled in Table 2.

4.5. Biological properties

Mg is one of the most important element constructed within the human body where it is involved in high number of enzymatic reactions. It was reported that Mg takes place in synthesis processes of protein and nucleic acid, stabilization of plasma membrane and many other cellular activities [47]. Amount of Mg in an average adult human body is around 21–28 g and more than 50% of which is present in bone tissue. Soft tissues contain 35–40% of this content and less than 1% is sequestered in serum [47]. Mg element, which is sequestered in bone, acts as a reservoir for acute change in Mg levels of serum.

Mg^{2+} bivalent ions play an important role in determining bone fragility. Also, it is known that Mg^{2+} ion takes place in transformation process of immature bone into a mature bone. Mg ion content in bone mineral is around 6 mol% but this content decreases during maturation process of bone. Cartilage and immature bone tissues contain high concentration of Mg^{2+} ion but this concentration changes depending on the aging. Moreover, presence of Mg in bone composition increases the elasticity of bone [47].

Effect of Mg on bone formation was investigated in previous studies. Presence of Mg has significant effect on osteoblastic cell differentiation. Bone formation around and over degraded Mg implants proved its effect on accelerating of bone healing. Mg degradation led to the release of Mg^{2+} ions to surrounding tissue which resulted in stimulation of local cells to bone formation. Also, it was proved that the hydrogen gas which is released during degradation process of Mg and its alloys can be tolerated by human body. However, high amount of hydrogen gas release can result in complication at healing period. Thus, the corrosion rate of Mg should be controlled to decrease risk of gas accumulation. The amount of gas cleared from the implantation site also depends on the implanted region and available blood flow [48].

Besides improving the mechanical properties and corrosion resistance, since Zn takes part in a wide range of physiological functions such as the regulation of immune system and enzymatic reactions, it was also reported that presence of Zn in composition of Mg alloys increases osteoblastic cell proliferation. However, high concentration of Zn resulted in cytotoxic effect in vitro. Hong et al. showed ZK40–Mg and AZ31–Mg increase cell proliferation in comparison to pure Mg. High concentration of corrosion products leads to

Table 2
Mechanical properties of powder processed Mg-based alloys.

Mg alloy	Tensile strength (MPa)	Yield strength (Mpa)	Elongation (%)	Young's Modulus (Gpa)	Compression strength (Mpa)	Bending strength (Mpa)	Reference
Mg–4.0Zn–0.2Ca (extruded)	297	240	21.3	45	–	–	[106]
Mg–Zn–Y–Nd (hot-extruded)	316	183	15.6	–	–	–	[107]
Mg–Zn–Y–Nd (CECed)	303	185	30.2	–	–	–	[107]
Mg–1.5Y–1.2Zn–0.44Zr (hot-extruded)	236	178	28	–	471	501	[109]
Mg–3Sn–0.5Mn	240	150	23	–	–	–	[102]
Mg–3Al–4Zn–0.2Ca	198	–	10.3	44.1	–	347	[97]
Mg–2Zn–0.5Ca–Mn (heat-treated)	205	–	15.7	–	–	–	[98]
Mg–5.3Zn–0.6Ca + 1.0Ce/La (extruded)	202	–	–	–	–	–	[99]
Mg–1Mn–2Zn–1.5Nd (extruded)	>285	–	>14	–	>395	–	[27]
Mg–**Gd**–Zn–Zr–Mn (extruded)	341	315	21.3	–	–	–	[105]
Mg–Gd–Nd–Zn–Zr (extruded)	267	217	–	–	–	–	[111]
Mg–Zn–Y–Nd (ECAP)	239	96	30.1	–	–	–	[108]
Mg–Zn–Y–Nd (CEC)	280	194	29.4	–	–	–	[108]
Mg–Zn–Y–Nd (extruded)	242	170	20.9	–	–	–	[108]

cytotoxic effect in human body due to osmotic shock effect on surrounding cells [49]. In another study, Mg implant which is alloyed with different amount of Al did not show any cytotoxic or neurotoxic effect up to 9 wt% of Al. Moreover, osteoblastic activity was increased with increasing amount of Al up to 9 wt% so the release of Al ions can be tolerated with human body at low levels [50].

Addition of Zr was also reported to improve the biocompatibility in vivo. Gu et al. showed that Zr higher than 5% led to unalloyed Zr phase in the alloy [51]. Unalloyed Zr phase led to a decrease in corrosion resistance so subsequently resulted in poor biocompatibility. As a result, the recommended content of Zr in Mg–xZr–ySr alloys was below 5% [52]. It was proved that the addition of Ca and Zr to Mg-based implants improve osseointegration rate and implant stabilization in host tissue [53].

4.6. Degradation

The corrosion of Mg and its alloys is an electrochemical process [112]. It is known that this process in aqueous environment is different than oxidation process in air [113]. The corrosion mechanism of Mg in aqueous environment can be explained with the following reactions [112–114].

$$Mg \rightarrow Mg^{2+} + 2e^{-} \quad \text{(Anodic reaction)} \tag{1}$$

$$2H_2O + 2e^{-} \rightarrow H_2 + 2OH^{-} \quad \text{(Cathodic reaction)} \tag{2}$$

$$2H_2O + O_2 + 4e^{-} \rightarrow 4OH^{-} \quad \text{(Cathodic reaction)} \tag{3}$$

$$Mg^{2+} + 2OH^{-} \rightarrow Mg(OH)_2 \quad \text{(Product formation)} \tag{4}$$

High amount of hydrogen gas evolution during anodic reaction resulted in decline of the speed of cathodic reaction which is known as negative difference effect phenomena [35,115]. The formation of moderately protective layer during cathodic reaction decreases cathodic reaction rate. However, these protective layers are not strong enough. Therefore, they break down before starting of anodic polarization [115].

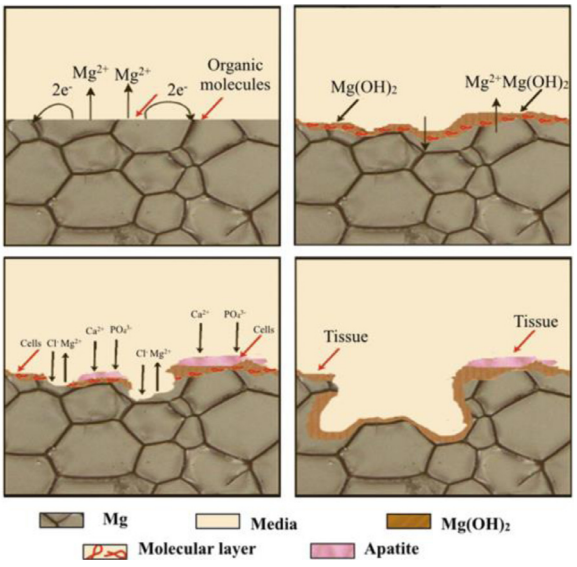

Fig. 1. Degradation mechanism of Mg in vivo [114].

Degradation behavior of Mg and its alloys are affected by different parameters such as aqueous environment, composition, structure, surface structure, alloying elements, impurities, secondary phase and manufacturing method [28,114].

Mg and its alloys show unpredictable behavior in physiological environment due to the presence of dissolved oxygen, proteins, amino acids, chloride and hydroxide ions (Fig. 1) [114,116]. Adsorption of amino acids, proteins and lipids over the surface alters the degradation rate of Mg and its alloys [114,116]. Also, $Mg(OH)_2$ acts as a protective layer which results in an increase in corrosion resistance. However, high concentration of chloride ions in physiological environments break down the protective layer of $Mg(OH)_2$ which leads to

pitting corrosion [10,117,118]. The corrosion mechanism of Mg in presence of chloride ions is explained as follows:

$$Mg\ (OH)_2 + 2Cl^- \rightarrow MgCl_2 \quad (5)$$

$$Mg + 2H_2O \rightarrow Mg(OH)_2 + H_2 \quad (6)$$

$$Mg + 2Cl^- \rightarrow MgCl_2 \quad (7)$$

Formation of $MgCl_2$ layer on the surface decreases the corrosion resistance since it is known that $MgCl_2$ is moderately soluble [10,117,118]. However, it is biocompatible and does not show any cytotoxic effect [10]. Furthermore, high concentration of hydroxyl ions in the environment increases the alkalinity and presence of calcium and phosphate ions leads to precipitation of calcium phosphate protective layer on the surface [114,119,120].

The presence of buffering agents such as HCl–Tris and Hepes which are used to neutralize pH value of SBF, accelerate corrosion rate of Mg-based implants by consuming OH^- ions [10]. Thus, consumption of OH^- ions leads to a decrease in corrosion product formation and an increase in corrosion rate. In contrast, protein (Fetal Bovine Serum) adsorption on the surface of Mg implants improves the corrosion resistance [10]. It is known that insoluble salts precipitate on the surface of Mg in presence of protein which form an insoluble dense layer on the surface. This protective layer improves the corrosion resistance [28,114].

It was reported that impurities and secondary phases play important role in corrosion resistance of Mg and its alloys. There is a difference between reference electrode potential of Mg and impurities/secondary phase which create micro-galvanic cell [28,35,113,117]. Corrosion rate of pure Mg increases in presence of impurities such as Fe, Ni, Cu and Co due to their higher standard electrode potentials [28]. It was accepted that secondary phase has significant effect on galvanic corrosion resistance of Mg and its alloys. Secondary phase can act as corrosion barrier or acts as a galvanic cathode [76,121,122]. Secondary phase amount, grain size, precipitation side and reference electrode potential should be taken into account to decide about its effect on corrosion rate [76,121,122]. It was reported that secondary phase with finer grain size precipitated along grain boundaries improve corrosion resistance while high corrosion potential of secondary phase increases the corrosion rate [122,123].

Corrosion behavior of Mg and its alloys is significantly affected by the microstructural defects such as dislocations and deformation twins [115]. An increase in residual stress as a result of microstructural defect, led to an increase in corrosion rate [115]. The corrosion rate of Mg and its alloys is increased due to an increase in population of dislocations, twins and grain boundaries. Also, mechanical stress has considerable effect on corrosion resistance.

Different types of corrosion are likely to occur in physiological environment [82]. Galvanic, intergranular, pitting and crevice corrosions are the most common types of corrosion. Galvanic corrosion is caused by the presence of two metals with different corrosion potentials at the same electrolyte. One of the metals acts as anode and the other one acts as cathode and form a galvanic couple [82]. Thus, anode metal is corroded due to electropotential difference between two metals. Probability of galvanic corrosion is high for Mg implants in physiological environment. The presence of different alloying elements and phases usually cause micro galvanic corrosion [124].

Pitting corrosion is commonly observed in environments with aggressive ions such as chloride ions in body fluid [125]. Pitting corrosion is occurred at regions adjacent to second phases in presence of chloride ions [125]. Fretting corrosion occurs on the contact surfaces of metals. This type of corrosion causing a mechanical wear should be considered for Mg-based metal implants [82]. The mechanism of crevice corrosion is similar to pitting corrosion and results in localized corrosion on the Mg implant surface. Microcracks can trigger crevice corrosion [82].

Corrosion resistance of Mg significantly changes by alloying element. Ca increases the corrosion resistance and decreases the grain size of the Mg alloys. Mg–Ca alloys containing different amounts of Ca are synthesized and it was proved that Mg alloy containing 0.6 wt% Ca gives better results in terms of corrosion resistance than other Ca compositions. Increasing the amount of Ca causes the formation of Mg_2Ca phase which lowers the corrosion resistance [126].

REEs are widely used in alloying of Mg to improve micro structure, mechanical properties and corrosion resistance. It was proved that REEs such as La and Gd improve corrosion resistance of biodegradable Mg alloys. However, the toxicity of the elements should be considered since good biocompatibility of the elements released by Mg alloys during degradation is essential for their use in an implant [127]. It was showed that mechanical properties of Mg alloys were improved by the addition of REEs due to the formation of metastable REEs containing phases along the grain boundaries [121]. Gd higher than 10% increases the mechanical strength because of noble behavior of Mg_5Gd precipitated in grain boundaries. Moreover, for Mg alloys containing 15% Gd, an increase in corrosion rate was observed. Addition of La to Mg alloys improves the corrosion resistance by forming a passive film [127]. However, there is no in vitro or in vivo investigation present on this alloy, which shows the lack of studies in this subject.

5. Computational studies on Mg alloys and its fabrication into implants

Computational models can be utilized to predict the mechanical function of biodegrading implants under physiological loading conditions as well as to understand interaction of implants with surrounding tissues. Design and manufacturing of Mg alloys are the other fields where computational models can be used to improve implant and stent designs as well as to optimize the operational parameters. Finite element models (FEM) have been used to predict deformation of

implants and their interaction with the surrounding tissues [128]. To determine the life-time and to assess the functionality of an implant, it is required to include extra modeling considerations e.g., corrosion behavior and change in mechanical strength of implant during healing period. Such models are still under development stage. For optimum design and functionality, existing empirical models for surface erosion and the related mass loss rate as well as mechanical characteristics under multi-axial load can be incorporated in computational models to predict biodegradation and change in mechanical strength of implants during healing. The following chapters review the literature related to computational studies of Mg alloys in an order consistent with the fields that they can be implemented.

5.1. Manufacturing processes

Computational models have been developed to investigate different aspects of manufacturing processes of Mg and Mg alloys. This could ease optimizing the process parameters as well as predicting the mechanical characteristics of Mg-based biomaterials.

One of the potential applications of Mg alloy can be in surgical threads. However, Mg alloys have low plasticity at RT, making the cold wire drawing process difficult. An experimental observation showed that the fracture of Mg alloys occurs in grain boundaries. Based on this, a mathematical damage model was developed [129]. Later on, a micro-scale numerical model was developed by Milenin et al. using the boundary element method (BEM) for the drawing process of MgCa0.8 alloy to optimize the deformation parameters based on the fracture in grain boundaries. The BEM model was then coupled with the authors' FEM code in order to model the wire drawing process at the macroscale. The developed wire drawing model can be used for both optimizing the parameters of the drawing process and predicting the ductility of the material [130].

In the cold production of Mg, low formability is one of the drawback. Combining the casting and forming processes within the horizontal twin-roll casting method can be a promising solution. This method involves feeding the molten Mg alloy between two counter rotating rolls which are water-cooled internally. The horizontal twin-roll casting of the Mg alloy AZ31 was numerically investigated using CFD model [131]. According to this study, cryogenic machining reduces the grain size of Mg alloy effectively and this grain refinement improves the corrosion resistance significantly. A preliminary study on modeling the microstructural changes of AZ31B Mg alloy during dry and cryogenic machining was conducted by Pu et al. using FE method and a user subroutine which is based on the dynamic recrystallization mechanism of Mg alloys. The model accurately predicted the experimental results [132].

The surface integrity in high-speed dry milling of biodegradable Mg–0.8Ca alloy was numerically investigated by Guo and Salahshoor. An internal state variability (ISV) model was used to model the inherent dynamic mechanical behaviors of high-speed cutting. A 2D FEA of plane strain orthogonal cutting was implemented using ABAQUS. Experimental and numerical studies revealed the same rake and relief angles of the rigid PCD tool. The predicted peak temperatures of the chips and machined surfaces were 600 and 400 °C, respectively. The surface temperature was sufficient to contribute to the formation of flank build-up. Predicted temperatures at the tool/chip interfaces were close to the melting temperature of the Mg–Ca0.8 alloy (650 °C) [133]. In another study, Split-Hopkinson pressure bar (SHPB) test was applied on Mg–0.8Ca alloy to observe the mechanical behavior of the biodegradable Mg–0.8Ca alloy under high strain rate loadings which is typical in metal cutting processes. Then the internal state variable (ISV) plasticity model was employed to model the material behavior under cutting regimes. A finite element (FE) analysis model was developed to study the chip formation during high speed dry cutting of MgCa0.8 alloy. Continuous chip formation predicted by FE simulation was verified by experimental results [134].

Another computational model was developed by Lin and Scott to determine the factors that contribute to the pull-out strength of the screws made of Mg and Mg alloy AZ31 implanted in a rabbit mandible. Holding strength of the screws, compared to the stainless steel screws, was measured in an in vitro pull-out test. Later, to simulate the pull-out test, a custom FE code was developed. All the screws that made of pure Mg, AZ31 and stainless steel exhibited very similar pull-out strength of around 40 N. Simulated pull-out force profiles indicated that for a constant diameter of the screw with similar interfacial conditions (e.g. depth of penetration, thread profile) the pull-out strength remains essentially constant. Then, the effect of the interfacial strength on the pull-out strength was examined keeping all the other model parameters constant. Predicted pull-out strength was increased with increasing interfacial strength. The study concluded that pull-out strength is highly sensitive on the interfacial strength between the screw and the bone, and it is insensitive to the modulus of the screw material [135].

Burnishing can be applied to improve the corrosion behavior of biodegradable MgCa0.8 alloy. An FE model was developed by Salahshoor and Guo to simulate contact mechanics in ball burnishing of MgCa0.8 biomaterial. The ISV plasticity model successfully predicted the mechanical behavior of MgCa0.8. The developed 2D axisymmetric FEM accurately predicted the dent geometry as well. Results of the study showed that the developed model is successful in predicting the large amount of compressive layers produced by small amount of shallow deformation which is the unique characteristics of ball burnishing [136].

In the reviewed literature, a variety of manufacturing processes such as drawing, casting, forming and burnishing have been numerically investigated for Mg-based materials. The developed models were successful in predicting the experimental results and optimizing the production parameters. These models help design and manufacturing of biodegradable Mg materials with desirable mechanical characteristics.

5.2. Degradation behavior

Uncontrolled degradation of biomaterials could result in loss of their mechanical integrity, metal contamination in the body and intolerable hydrogen evolution by tissue. Computational studies on degradation behavior of Mg-based implant and stent materials provide researchers with a clear information of the relevance of several factors to corrosion rate, significant parameters for a reliable in vitro testing, and general corrosion behavior of biodegradable stents and implants. These could also contribute saving time and energy required for the experimental research.

5.2.1. Degradation behavior of implants

Mg-based glasses are reported to offer extended solubility period for alloying elements and a homogeneous single-phase structure, both of which can contribute improving corrosion behavior of the biomaterial significantly. The reduction of hydrogen evolution in biodegradable Zn-rich MgZnCa glasses was studied by Zberg et al. It was observed that above a particular Zn-alloying threshold (28 wt%), a Zn- and oxygen-rich passivating layer forms on the surface of the alloy which prevents rapid corrosion of the material. A model was developed based on the calculated Pourbaix diagram of Zn in SBF using corrosion analyzer software [137]. The relevance of several parameters to the corrosion rate of biodegradable Mg was investigated by Willumeit et al. through artificial neural network (ANN) analysis. The results showed that the most significant parameters to be included for reliable in vitro tests are CO_2 and NaCl [138]. Another study investigated the degradation of Mg due to the presence of impurities and the thickness of electrolyte using the FE method. The results showed that Mg implant covered by a thick layer of electrolyte suffers severe corrosion attack, but this is significantly reduced when a thin enough layer is formed on Mg [139].

Preliminary in silico assessment of the degradation rate of Mg implant would save the time required for in vitro analysis. A new partial differential equation (PDE) model for the chemistry of corrosion was developed by Bajger. He used the hydrogen evolution rate data obtained from an immersion test of pure Mg in SBF to calibrate the PDE model [140]. Another mathematical model for the corrosion behavior of Mg was developed by Bajger et al. to aid the design of biodegradable implants with suitable geometries. Level-set method was employed to track complicated geometries as it is the case of porous implants. The study provided a framework for the assessment of the corrosion rate of Mg including the formation and dissolution processes of the protective film [141]. The corrosion rate of Mg–Zn–RE–xCa alloy with Ca contents varying from 0 to 6 wt% was experimentally and theoretically evaluated by Bakhsheshi-Rad et al. and the experimental results were compared with the simulation results. Good agreement in terms of corrosion rate was found between experimental and predicted results [120].

5.2.2. Degradation behavior of stents

A new design concept of Mg alloy stent was proposed by Wu et al. and a shape optimization method with FE analysis on 2D stent models was applied considering four different Mg alloys namely; AZ80, AZ31, ZM21, and WE43. The optimized designs were compared with an existing Mg alloy stent design by 3D FE analysis. The results showed that the optimized design with alloy WE43, compared to the existing Mg alloy stent, had an increased strut width by approximately 48%, improved safety properties (reduced the maximum principal stress after recoil with tissue by 29%, and reduced the maximum principal strain during expansion by 14%) and improved scaffolding ability by 24%. Accordingly, the degradation time can be expected to extend. The applied methodology was suggested to provide a convenient and practical way to develop novel Mg alloy stent designs [142].

The first computational study to predict the interaction between Mg alloy stent and arterial tissue was carried out by Wu et al. Due to short degradation time, Mg alloy stents exhibit insufficient scaffolding to the target vessels. Aiming to improve the design and degradation behavior of Mg alloys, Wu et al. developed a degradable FEM for Mg alloy stents. A three dimensional FEM was combined with degradable material model of AZ31 and applied to stents of conventional and optimized designs. These designs were implanted through simulation into a vessel model and degraded by changing interactions between outer stent surface and the vessel. The 3D model was suggested to provide a proper design and testing tool for novel Mg alloy stents [143]. Following the development of FEM for degradable Mg alloy stents, the model was experimentally validated with twelve Mg alloy stents by Wu et al. Six samples were designed according to the developed degradation model and the other six samples were conventionally designed. The experimental results showed that the samples of the optimized design had better corrosion resistance than those of the conventional design. The degradation process of the samples was dominated by uniform and stress corrosion [144]. This experimental work was the first validation of the computational approach, which can be utilized to design, test and improve Mg alloy stents.

Another computational model was developed to predict degradation rate of Mg that can be utilized in bioresorbable stent design. Continuum damage mechanics (CDM) model was used to model the loss of mechanical strength of the material by occurrence of geometrical discontinuities. For that purpose, a scalar field was defined to quantify the damage distribution. The developed model was then implemented in FE framework. Two mechanisms were considered for corrosion of Mg; stress corrosion and galvanic corrosion. Galvanic corrosion was used to describe mass loss when the material is exposed to an aggressive environment, even in a stress-free zone. On the other hand, stress corrosion accounted for the damage due to the localization of the corrosion attack in the zones of concentrated stress [145].

The influence of degradation on the mechanical integrity of Mg stents was numerically modeled by Grogan et al. In order

to analyze the corrosion in complex 3D geometries, a phenomenological corrosion model was developed and applied within an FE framework. An element-specific dimensionless pitting parameter was introduced to include the heterogeneous or pitting corrosion to the modeling framework. Results of the study suggested that the developed model can be used to predict the performance of a bioabsorbable stent placed in an artery [146]. Development of an implicit FE solution method allowed to reduce the simulation time and extend the applicability of degradation models of Mg stents. The developed strategy was successful in predicting the localized corrosion of stent struts for progressively more complex vessel-stent patterns [147].

The expanding rates, Poisson's ratio and deformation behavior of self-expanding auxetic stents of different geometries were modeled and simulated by Carneiro and Puga. The results of the study indicated that Reentrant and Chiral geometries exhibit low Poisson's ratio and high expanding rates. Moreover, the observed deformation behavior implied a less axial deformation [148]. A computational test-bed for stent angioplasty was developed by Boland et al. to simulate stent tracking, balloon expansion, recoil and in vivo loading in an atherosclerotic artery model. A corrosion model was also developed to simulate uniform and pitting corrosion of Mg stent as well as its interaction with arterial tissue. The study revealed a growth of new arterial tissue around the stent struts that has a significant influence on the mechanical behavior of the degrading stent [149].

Compared to the implants, stents typically have more complex geometries. In the discussed literature, extended stent degradation periods have been attained with the proposed models that allow shape optimization for stent design. Moreover, these models bring about improved mechanical strength and improved scaffolding ability of stents. Additional models have been proposed to observe the interaction of Mg alloy stent with arterial tissue as well as to predict the degradation rate and performance of Mg stents.

6. Mg-based composites for potential biomedical implant applications

Biodegradability of Mg alloys makes them suitable for orthopedic implants. Many studies indicated that designing Mg alloys with controllable degradation rates is highly demanded. Development of new composites based on Mg alloys with other systems could be a promising solution to meet this demand [150]. Researchers have incorporated different type of ceramic and polymer materials with Mg and Mg alloys to form Mg-based composites through various manufacturing routes and investigated their effect on corrosion resistance, mechanical properties and biocompatibility. In ceramic composites, Mg and Mg alloys are used as the matrix and the matrix is reinforced by ceramics whereas in polymer composites Mg and Mg alloys are usually added to reinforce the polymer matrix.

6.1. Mg-polymer composites

Expecting the polymer matrix to benefit from the higher strength and modulus of the Mg particles as well as Mg to benefit from the surrounded protective polymer matrix that can improve the corrosion resistance, Cifuentes et al. developed a poly-L-lactic acid (PLLA)/Mg composite. Composite specimens were prepared by combining solvent casting of PLLA loaded with 30 wt% Mg particles and further molding by compression. Reinforcing the polymer matrix with Mg particles improved Young's modulus up to 8 GPa, YS up to 100 MPa and hardness up to 340 MPa [151]. In order to test the suitability of different methods to fabricate PLLA/Mg composites, hot extrusion was employed. Extrusion distributed Mg particles uniformly within PLLA matrix. Addition of Mg up to 5% increased the degradation rate slightly, but significant increment was observed at 7%. Similarly, mechanical strength of the specimen increased by addition of Mg up to 5%, but it dropped drastically after the Mg content reached to 7% [152].

To improve the mechanical properties of PLLA polymer and to prevent its inflammatory response in biomedical applications Kum et al. developed a hybrid composite by incorporating oligolactide-grafted magnesium hydroxide (Mg-OLA) in a biodegradable polymer matrix (PLLA). Mg-OLAs were synthesized using ring opening polymerization method. The measured UTS and modulus of PLLA/Mg80-OLA20 (0–20 wt%) were higher than PLLA/magnesium hydroxide. Increasing the amount of Mg80-OLA20 from 0 to 20 wt% increased the cell viability by 100% that appeared to have a positive effect on cytotoxicity as well as inflammatory response of the composite [153].

Reinforcement of poly lactic-co-glycolic acid (PLGA) by Mg alloy AZ31 was studied by Wu et al. Addition of AZ31 fibers significantly enhanced the UTS and elongation of the composite. The acid degradation products of PLGA were neutralized by the alkaline corrosion products of AZ31 Mg alloy fibers. Direct cell attachment test showed that all the cells exhibi a healthy morphology and the cells adhesion and proliferation on the specimen surface were observable [154]. Brown et al., for the first time, developed a metallic Mg particle/PLGA composite scaffold using a solvent casting, salt leaching method to enhance bone regeneration after tooth extraction. By addition of Mg into the PLGA scaffolds the compressive strength and modulus were increased, and a suitable porous structure was obtained for cell infiltration. Combining basic-degrading Mg with acidic-degrading PLGA led to an overall pH buffering effect and a long-term release of Mg over the period of 10-week degradation assay. Degradation products of Mg/PLGA composite scaffolds increased the proliferation of bone marrow stromal cell in vitro. Histological analysis indicated that the composite is biologically safe [155].

It is apparent from the discussed literature that reinforcing Mg enhances mechanical properties of the biopolymer matrix. Also, the corrosion resistance of Mg improves when it forms composites with polymer matrix. However, the resulting

mechanical strength of the composites is usually below that of Mg. Thus, more research can be conducted to develop and identify composites of Mg with biopolymers within a range of acceptable mechanical strength.

6.2. Mg-ceramic composites

Composites made up of various Mg alloys as matrix and various ceramics as reinforcements, with different fabrication routes have been extensively investigated to assess their viability in biomedical applications. A group of biomaterials which have similar characteristics with the mineral parts of bone seems very promising for hard tissue engineering applications. This group includes calcium phosphates, especially HAp, beta-tricalcium phosphate (β-TCP) and bicalcium phosphate (BCP) which is the combination of HAp and β -TCP [150]. Calcium phosphates induce adsorption of ions and deposition of calcium phosphate minerals on the composite surface which stimulate the bone growth. However, their mechanical properties cannot compete with that of bone. A possible solution to this could be procured through development of calcium phosphates composites with Mg and Mg alloy matrix. Research groups evaluated the incorporation of HAp into pure Mg and Mg alloys such as AZ91D and MgCa. A metal matrix composite (MMC) composed of Mg alloy AZ91D matrix and HAp reinforcements was fabricated by Wittea et al. through hot extrusion. Mechanical properties of the composite were found to be very similar to that of the natural bone. HAp particles stabilized the corrosion rate and exhibited more uniform corrosion attack in artificial sea water and cell solutions. During immersion test, the bone cells were able to adhere, proliferate and survive on the surface of MMC-HA composite [156]. Chen et al. used AZ91 Mg alloy and porous HAp to prepare AZ91/HAp composite through squeeze casting method. A significantly higher compressive strength was observed with AZ91/HAp composite compared to HAp. AZ91 alloy exhibited a lower corrosion resistance in comparison with HAp. Therefore, it can lead recurrence of the porous HAp and promote bone cell adhesion and proliferation [157].

Compared to casting methods, PM is reported to be a more suitable method to obtain homogeneous distribution of ceramic particles in Mg matrix [150]. Hence, PM method was employed by Gu et al. to fabricate Mg/HAp composites of varying HAp content (10 wt%, 20 wt% and 30 wt%). Mg/10HAp composite showed a uniform HA particle distribution. Compared to the as-extruded bulk pure Mg, an enhanced YS but reduced UTS and elongation was observed with Mg/10HAp composite. Increasing HAp content also increased the corrosion rate of the composite. The cytotoxicity evaluation showed that Mg/10HAp is compatible to L-929 cells [158]. Friction stir processing method was employed by Sunil et al. to synthesize n-HAp-reinforced Mg composite Mg–nHAp. The applied method refined grain size from 1500 μm to as low as 3.5 μm. Addition of nHA and the refined grain size improved biomineralization in SBF. Cytotoxicity study indicated only a marginal increase in cell viability of the Mg–nHAp composite. The composite exhibited a superior cell adhesion [159].

Microwave assisted sintering method was used Xiong et al., for the first time, to prepare HAp-reinforced Mg composites. Microscopic evaluations showed a homogenous distribution of HAp particles in Mg matrix. Significantly improved mechanical properties (flexural strength and modulus and compressive strength and modulus), enhanced corrosion resistance, superior cytocompatibility and bioactivity were achieved with HAp/Mg compared to that of the pure Mg. It was concluded that the HAp content has control over mechanical properties, corrosion resistance and biological behavior of HAp/Mg composite [21].

Mg alloy (ZK60A) matrix composites reinforced with varying contents of calcium polyphosphate particles were fabricated by Feng and Han through PM. A uniform particle distribution of polyphosphate in the ZK60A matrices without voids were observed in the composites containing 2.5 wt% and 5 wt% calcium polyphosphate. Mechanical properties (UTS, YS and elastic modulus) and corrosion rate of the composite were adjustable with the control of calcium polyphosphate content. $Mg(OH)_2$ formation on the composite surface was observed after immersion of the samples into physiological saline solution [160]. An MMC of HAp/Mg–Zn which is composed of Mg alloy Mg–Zn as matrix and different concentrations of thermal-treated HAp particles as reinforcements was fabricated by Liu et al. The addition of HAp particles altered the corrosion mechanism of Mg matrix. During the corrosion process, HAp particles adsorbed PO_3^{-4} and Ca^{2+} ions efficiently and Ca-P compounds were deposited on the surface of composites. HA slowed down the corrosion rate of Mg matrix composites in SBF. It is also indicated that Zn addition improves the corrosion behavior of HAp/Mg composites [161]. A Mg MMC was synthesized by Ye et al. using Mg–2.9Zn–0.7Zr alloy as the matrix and 1 wt% n-HAp particles as reinforcements. The composite exhibited a lower rate of corrosion and more favorable in vitro cytocompatibility in comparison with the Mg–Zn–Zr alloy. Composite surface was covered with white Ca–P precipitates. Electrochemical test results revealed that the addition of n-HAp particles increases the corrosion potential. An adhesion and proliferation of cells on the surface of the composite was observed. The results of Mg–Zn–Zr/n-HAp composite were promising to be considered as biodegradable bone fixation material [162]. Nanofluorapatite-reinforced AZ91 Mg alloy composite was synthesized by Razavi et al. through blending–pressing–sintering method. The addition of fluorapatite nanoparticles to Mg alloys enhanced the mechanical properties and corrosion resistance, and accelerated the formation of an apatite layer on the surface, which contributed to the protection of AZ91 matrix and enhanced osteoconductivity of Mg alloys for biomedical applications [163,164].

β-TCP ($Ca_3(PO_4)_2$) is another calcium phosphate used in bone substitution. Compared to HAp, it is bioresorbable in biological environment and it shows osteoinductive properties. Despite the rapid dissolution of β -TCP and Mg, their composites revealed favorable degradation rates. He et al.

added β-TCP particles into Mg–Zn–Zr alloy to improve its microstructure and properties through hot extrusion process. Mg–Zn–Zr/β-TCP composite grains were considerably refined. Addition of β-TCP as well as the obtained fine grain size enhanced the UTS and the elongation of the composite. The corrosion resistance of the composites was considerably improved compared to that of Mg–Zn–Zr alloy [165]. Suction casting method was employed by Wang et al. to fabricate β-TCP/Mg–Zn–Mn composite through infiltrating Mg–Zn–Mn alloy into porous β-TCP. A compact structure and a good interfacial bonding between Mg–Zn–Mn alloy and β-TCP scaffold were obtained. An UTS of 140 ± 20 MPa similar to the bone and 1000-fold higher than porous β-TCP scaffold was attained. The composite possessed an improved corrosion resistance compared to the Mg–Zn–Mn alloy. The corrosion products ($Mg(OH)_2$, $Ca_3(PO_4)_2$ and HAp) on the composite surface were desirable compounds for bone growth [166].

A β-TCP /Mg–Zn composite was fabricated by Yu et al. using PM. The density and elastic modulus of the β-TCP /Mg–6%Zn composite matched well with those of natural bone, and the strength was approximately double that of natural bone. 10% β-TCP/Mg–Zn exhibited a favorable corrosion resistance and the in vitro cytotoxicity evaluation revealed a cytotoxicity grade of 0–1 against L929 cells meaning the composite is safe for cellular applications. β-TCP/Mg–Zn composite also exhibited a good biocompatibility with the tissue and visceral organs. The composite was found to have a proper degradation rate and improved healing of a pre-broken leg. The corrosion products were $Mg(OH)_2$ and $Ca_5(PO_4)_6(OH)_2$ which are known to advance the biocompatibility [167]. Yu et al. also fabricated Mg–6%Zn–15% β-TCP composite again through PM and investigated its biocompatibility and biodegradation in vivo. The composite was implanted to the pre-broken femoral shaft of a rabbit model. Throughout the experiment Mg^{2+}, Zn^{2+}, Ca^{2+} ion concentrations were in the normal range in animal's blood. Inspections of the visceral organs during composite degradation showed no anomaly signifying good biocompatibility. Biodegradation of the composites induced growth of the bone tissues [168]. The results of these studies suggested that owing to its good biocompatibility and suitable biodegradation characteristics, the optimum composition of the Mg–$Ca_3(PO_4)_2$ composite could be a good candidate for implant materials.

An ideal biodegradable material should gradually dissolve concurrently with the process of newly forming bone. Biphasic calcium phosphate (BCP) can be a promising choice which is a biomaterial comprising different proportions of HAp and β-TCP. An appropriate proportion can allow obtaining desirable degradation rates. Despite excellent biocompatibility and degradation rates, BCP lacks required mechanical strength [150]. The strength of bicalcium phosphate (BCP) scaffold was enhanced as much as 200-fold, corresponding to the half of the strength of bulk MgCa alloy, by forming MgCa-HAp/TCP composite through incorporation of MgCa alloy. Slower corrosion rate was obtained with MgCa-HAp/TCP composite compared to the bulk MgCa alloy. In addition, the cytotoxicity evaluation showed Mg/10HAp composite extraction medium did not induce toxicity to L-929 cells [169].

Composites of Mg with silica and silicate materials also exhibited enhanced mechanical properties and bioactivity as well as reduced degradation rate. A semi-solid high pressure casting process was applied by Huan et al., for the first time, to incorporate bioactive glass (BG, 45S5) particles into Mg alloy (ZK30). The bioactive glass particles were observed to distribute uniformly in ZK30 matrix. Compared to the ZK30 alloy, the composites had an improved ability to induce the formation of a bone-like apatite layer on the surface, indicating an enhanced surface biocompatibility [170]. The composite showed a lower rate of degradation and hydrogen evolution than the matrix alloy. In vitro cytotoxicity evaluation of the composite revealed ionic products of degradation have superior ability to support the survival, proliferation, and osteoblastic differentiation of bone marrow stromal cells to those of the ZK30 alloy [171].

A bioceramic-based composite was fabricated by mixing HAp and bioactive glass ($64SiO_2$–26CaO–5MgO–5ZnO (based on mol%)) powders through sintering method. Maintaining the sample for 14 days in SBF decreased its compressive strength by 65%. In addition to its cytocompatibility confirmed through in vitro biological evaluation, significant release of silicon ions in SBF was interpreted as the sign of osteoinductivity [172]. In another study, an MMC made up of pure Mg as the matrix and bioceramic calcium silicate (CS) as the reinforcement was synthesized by Huan et al. using SPS method. The addition of calcium silicate particles improved the compressive strength of Mg matrix by 30%. Immersion test in SBF showed that the corrosion resistance of Mg was improved owing to the accelerated precipitation of HAp on the composite surface. Release of Si ions from the calcium silicate phase enhanced the ability of the composite to stimulate the ALP expression of osteoblast-like cells compared to pure Mg [173]. An Mg matrix composite reinforced by bredigite was developed by Dezfuli et al. A 67% higher ultimate compressive strength and an improved ductility by 111% were achieved through incorporating 20 vol% bredigite particles in Mg matrix. The in vitro degradation rate of the Mg-20% bredigite composite was observed as 24 times lower than that of monolithic Mg. Therefore, after 12 days of immersion in the cell culture medium, the mechanical properties of the composite were still comparable to those of cortical bone [174].

Many researches were performed to investigate the Mg composites reinforced by MAX phases. The "MAX phases" are applied to a family of more than 60 ternary nitrides and carbides that share a layered structure. The term "MAX" represents the formula $M_{n+1}AX_n$, where $n = 1$, 2, or 3, M is an early transition metal, A is an A-group element (specifically, the subset of elements 13–16) and X is carbon and/or nitrogen. The $M_{n+1}AX_n$ layers are characterized by strong covalent M–X bonds interleaved with A layers through weaker M–A bonds. This inherent nano-layered structure provides a unique combination of metal-like and ceramic-like properties [175]. They are elastically rigid (Young's moduli > 300 GPa)

with low density (4 g/cm^3), chemically inert, good thermal and electrical conductors, and have relatively low thermal expansion coefficient. They are relatively soft and most are readily machinable, resistant to fatigue and thermal shock [176]. Yu et al. [175] fabricated Ti2AlC-reinforced AZ91D composites by stir casting method. After reinforcement, higher values of YS, UCS and Young's moduli were obtained and these values increased with increasing Ti2AlC volume fraction. The Amini and Barsaum [175] achieved a very high UCS value of 800 MPa with MAX phase reinforced Mg composites (Mg/Ti2AlC 50:50 vol%) made through hot pressing. Despite many potential advantages of MAX phases reinforced Mg matrix composites, to the best of authors' knowledge, there is no published work in the literature which investigate their application in biomedical field. Thus, this field requires further studies including synthesis and characterization of MAX phases-reinforced Mg matrix composites for their biocompatibility and biodegradation performance.

In the above discussed literature several ceramic reinforcement phases with different methods of production have been proposed for synthesis of Mg matrix composites in order to achieve the required enhancements in Mg-based implant materials. These composites have exhibited characteristics of high strength, low corrosion rate and enhanced bioactivity compared to that of available Mg alloys, making them promising candidates to be used as biomaterials.

7. Summary, conclusions and recommendations

The present paper is a comprehensive, comparative and critical review of the recent literature on synthesis and performance evaluation of various types of Mg-based biomaterials. Mg degrades in physiological environment without dissipating any toxicity. Therefore, it eliminates the need of a secondary surgical operation for implant removal provided that its degradation rate is harmonized with the tissue healing rate. Several synthesis methods have been implemented to synthesize Mg-based biomaterials with different type of material components. The main target was to achieve a controllable degradation. In this regard, after synthesis, in vitro and in vivo studies have been conducted. In addition, performances of the materials and synthesis processes have been evaluated through computational studies.

Among the available synthesis methods, PM appears as the most favorable method. It could produce interconnected porous microstructures with desired pore size and distribution which is essential for an enhanced biological interaction of the materials and implanted environment. PM also produces finer grain size and suppresses the formation of secondary phase during synthesis. Besides, it is required to optimize the PM process parameters to synthesize biomaterials with desired characteristics.

Beside the microstructure, the role of materials surface characteristics is vital for biocompatibility. Textured surfaces improve the cell attachment and proliferation. Thus, mimicking the natural bone surface with both nano- and microtextures is suggested to promote osteointegration.

Alloying of Mg, and forming of Mg composites with ceramics and polymers by using several synthesis methods have been studied to enhance the mechanical properties and corrosion resistance of Mg. Mg has been alloyed with different metals at different concentrations. Researchers have reported that there are certain concentration limits for the alloying elements, above which they are toxic to the biological environment and they can adversely affect mechanical properties of the materials.

Low ductility of Mg is the limitation since usually the surgeon needs to bend the fixture to fit it to the hard tissue properly. In addition, the stent material should be ductile enough to allow forming of complex structure. Researchers have identified alloying elements that improve the ductility of Mg without having a significant effect on mechanical strength.

Synthesis processes and degradation behavior of Mg-based biomaterials have been studied in silico. The developed models allow to improve implant and stent design by optimizing the process parameters. The models also accurately predict the degradation rate of biomaterials and their interaction with surrounding tissues.

Enhanced corrosion resistance, biocompatibility and mechanical properties have been attained by the composites of Mg and Mg alloys. The corrosion resistance of Mg improves when it forms composites with polymer matrix. Also, Mg reinforcement enhances the poor mechanical properties of polymers. However, mechanical properties of the resultant composites are insufficient for hard tissue applications. On the other hand, several ceramic reinforcement phases with different methods of production have been proposed for synthesis of Mg matrix composites in order to achieve the required enhancements in Mg-based biomaterials. These composites have exhibited characteristics of high strength, low corrosion rate and enhanced bioactivity compared to that of available Mg alloys, making them promising candidates to be used as biomaterials. Knowing the potential advantages of MAX Phases reinforced Mg matrix composites, they should be investigated for biomedical applications.

Previous investigations proved that the main drawback of pure Mg and its alloys is corrosion rate and unpredictable behavior in body fluid. In vivo tests are a must for further understanding of their behavior in a living system. A systematic and comprehensive approach to achieve well-controlled and durable material properties is needed to compensate unpredictable nature of living systems. Also, the morphology and hierarchical structure of bone should be taken into account in design of implants to improve bone and implant integrity. As explained above, surface roughness is one of the most significant factors in cell attachment and corrosion rate of Mg and its alloys. However, there is not sufficient number of investigations on it. Thus, the effect of surface roughness on corrosion behavior should be comprehensively investigated in silico, in vitro and in vivo conditions. Furthermore, the effect of surface morphology and porosity on degradation rate of Mg implants in living systems has not been completely investigated. Also, the manufacturing method plays important role in final properties of Mg-based implant. There is a

need to select a method to achieve desirable surface roughness, porosity, corrosion resistance and mechanical properties at the same time. In this matter, further computational studies are required.

Future studies are also recommended to mimic the bone surface by creating combined nano- and micro-textures and investigate the synthesis of Mg-based non-toxic materials by making standards through identifying the biologically safe elements and safety limits for the elements' concentration.

References

[1] A. Tahmasebifar, S.M. Kayhan, Z. Evis, J. Alloys Compd. 687 (2016) 906–919.
[2] B.D. Ratner and B.S. An, "Biomaterials Science: An Introduction to Materials in Medicine," vol. 26, p. 5093, 2005.
[3] S. Wu, X. Liu, K.W.K. Yeung, H. Guo, P. Li, T. Hu, C.Y. Chung, P.K. Chu, Surf. Coat. Technol. 233 (2013) 13–26.
[4] A. Biesiekierski, "A New Look at Biomedical Ti-based Shape Memory Alloys," no. January 2012, 2012.
[5] Y. Chen, Z. Xu, C. Smith, J. Sankar, Acta Biomater. 10 (11) (2014) 4561–4573.
[6] S.V. Dorozhkin, Acta Biomater. 10 (7) (2014) 2919–2934.
[7] N.E.L. Saris, E. Mervaala, H. Karppanen, J.A. Khawaja, A. Lewenstam, Clin. Chim. Acta 294 (1–2) (2000) 1–26.
[8] A. Biesiekierski, J. Wang, M. Abdel-Hady Gepreel, C. Wen, Acta Biomater. 8 (5) (2012) 1661–1669.
[9] J. Li, L. Tan, P. Wan, X. Yu, K. Yang, Mater. Sci. Eng. C 49 (June) (2015) 422–429.
[10] Y.F. Zheng, X.N. Gu, F. Witte, Mater. Sci. Eng. R Rep. 77 (2014) 1–34.
[11] J. Cheng, B. Liu, Y.H. Wu, Y.F. Zheng, J. Mater. Sci. Technol. 29 (7) (2013) 619–627.
[12] J. Lévesque, H. Hermawan, D. Dubé, D. Mantovani, Acta Biomater. 4 (2) (2008) 284–295.
[13] M. Peuster, C. Hesse, T. Schloo, C. Fink, P. Beerbaum, C. von Schnakenburg, Biomaterials 27 (28) (2006) 4955–4962.
[14] J.M. Seitz, A. Lucas, M. Kirschner, JOM 68 (4) (2016) 1177–1182.
[15] H. Ibrahim, S.N. Esfahani, B. Poorganji, D. Dean, M. Elahinia, Mater. Sci. Eng. C 70 (2016) 870–888.
[16] N. Li, Y. Zheng, J. Mater. Sci. Technol. 29 (6) (2013) 489–502.
[17] W. Schmidt, P. Behrens, C. Brandt-Wunderlich, S. Siewert, N. Grabow, K.P. Schmitz, Cardiovasc. Revascularization Med. 17 (6) (2016) 375–383.
[18] H. Windhagen, K. Radtke, A. Weizbauer, J. Diekmann, Y. Noll, U. Kreimeyer, R. Schavan, C. Stukenborg-Colsman, H. Waizy, Biomed. Eng. Online 12 (1) (2013) 62.
[19] G. Xie, H. Takada, H. Kanetaka, Mater. Sci. Eng. A 671 (2016) 48–53.
[20] A.K. Chaubey, S. Scudino, M. Samadi Khoshkhoo, K.G. Prashanth, N.K. Mukhopadhyay, B.K. Mishra, J. Eckert, J. Alloys Compd. 610 (2014) 456–461.
[21] G. Xiong, Y. Nie, D. Ji, J. Li, C. Li, W. Li, Y. Zhu, H. Luo, Y. Wan, Curr. Appl. Phys. 16 (8) (2016) 830–836.
[22] J. Feng, H. Sun, X. Li, J. Zhang, W. Fang, W. Fang, Adv. Powder Technol. 27 (2) (2015) 550–556.
[23] M. Rashad, F. Pan, W. Guo, H. Lin, M. Asif, M. Irfan, Mater. Charact. 106 (2015) 382–389.
[24] D. Yang, Z. Hu, W. Chen, J. Lu, J. Chen, H. Wang, L. Wang, J. Jiang, A. Ma, J. Manuf. Process. 22 (2016) 290–296.
[25] M.H. Kang, H. Do Jung, S.W. Kim, S.M. Lee, H.E. Kim, Y. Estrin, Y.H. Koh, Mater. Lett. 108 (2013) 122–124.
[26] H. Asgharzadeh, E.Y. Yoon, H.J. Chae, T.S. Kim, J.W. Lee, H.S. Kim, J. Alloys Compd. 586 (SUPPL. 1) (2014) S95–S100.
[27] Y.L. Zhou, Y. Li, D.M. Luo, Y. Ding, P. Hodgson, Mater. Sci. Eng. C 49 (2015) 93–100.
[28] X. Li, X. Liu, S. Wu, K.W.K. Yeung, Y. Zheng, P.K. Chu, Acta Biomater. 45 (2016) 2–30.
[29] Y. Bi, Y. Zheng, Y. Li, Mater. Lett. 161 (2015) 583–586.
[30] Z.S. Seyedraoufi, S. Mirdamadi, J. Mech. Behav. Biomed. Mater. 21 (2013) 1–8.
[31] M. Yazdimamaghani, M. Razavi, D. Vashaee, K. Moharamzadeh, A.R. Boccaccini, L. Tayebi, Mater. Sci. Eng. C (71) (2016) 1253–1266.
[32] R. del Campo, B. Savoini, A. Muñoz, M.A. Monge, G. Garcés, J. Mech. Behav. Biomed. Mater. 39 (2014) 238–246.
[33] S. Cabeza, G. Garcés, P. Pérez, P. Adeva, J. Mech. Behav. Biomed. Mater. 46 (2015) 115–126.
[34] S.Z. Khalajabadi, M.R. Abdul Kadir, S. Izman, M. Marvibaigi, J. Alloys Compd. 655 (2016) 266–280.
[35] A. Tahmasebifar, S.M. Kayhan, Z. Evis, A. Tezcaner, H. Çinici, M. Koç, J. Alloys Compd. 687 (2016) 906–919.
[36] S.M. Kayhan, A. Tahmasebifar, M. Koc, Y. Usta, A. Tezcaner, Z. Evis, Mater. Des. 93 (2016) 397–408.
[37] X.C. Xia, X.W. Chen, Z. Zhang, X. Chen, W.M. Zhao, B. Liao, B. Hur, J. Magnes. Alloy. 1 (4) (2013) 330–335.
[38] M. Yazdimamaghani, M. Razavi, D. Vashaee, L. Tayebi, Mater. Sci. Eng. C 49 (2015) 436–444.
[39] M. Wolff, J.G. Schaper, M.R. Suckert, M. Dahms, T. Ebel, R. Willumeit-Römer, T. Klassen, JOM 68 (4) (2016) 1191–1197.
[40] B. Ratna Sunil, C. Ganapathy, T.S. Sampath Kumar, U. Chakkingal, J. Mech. Behav. Biomed. Mater. 40 (2014) 178–189.
[41] J. Zhang, Z. Kang, F. Wang, Mater. Sci. Eng. C 68 (2016) 194–197.
[42] R. Viswanathan, N. Rameshbabu, S. Kennedy, D. Sreekanth, K. Venkateswarlu, M. Sandhya Rani, V. Muthupandi, Mater. Sci. Forum 765 (Jul. 2013) 827–831.
[43] M.-H. Kang, T.-S. Jang, S.W. Kim, H.-S. Park, J. Song, H.-E. Kim, K.-H. Jung, H.-D. Jung, Mater. Sci. Eng. C 62 (2016) 634–642.
[44] H. Gong, B. Anasori, C.R. Dennison, K. Wang, E.C. Kumbur, R. Strich, J.G. Zhou, J. Mater. Sci. Mater. Med. 26 (2) (2015) 110.
[45] K. Kowalski, M. Nowak, J. Jakubowicz, M. Jurczyk, J. Mater. Eng. Perform. 25 (10) (2016) 4469–4477.
[46] Y. Wan, T. Cui, W. Li, C. Li, J. Xiao, Y. Zhu, D. Ji, G. Xiong, H. Luo, Mater. Des. 99 (2016) 521–527.
[47] J. Walker, S. Shadanbaz, T.B.F. Woodfield, M.P. Staiger, G.J. Dias, J. Biomed. Mater. Res. – Part B Appl. Biomater. 102 (6) (2014) 1316–1331.
[48] A. Chaya, S. Yoshizawa, K. Verdelis, N. Myers, B.J. Costello, D.-T. Chou, S. Pal, S. Maiti, P.N. Kumta, C. Sfeir, Acta Biomater. 18 (2015) 262–269.
[49] D. Hong, P. Saha, D.-T. Chou, B. Lee, B.E. Collins, Z. Tan, Z. Dong, P.N. Kumta, Acta Biomater. 9 (10) (2013) 8534–8547.
[50] F. Witte, V. Kaese, H. Haferkamp, E. Switzer, A. Meyer-Lindenberg, C.J. Wirth, H. Windhagen, Biomaterials 26 (17) (2005) 3557–3563.
[51] X.N. Gu, N. Li, Y.F. Zheng, L. Ruan, Mater. Sci. Eng. B Solid-State Mater. Adv. Technol. 176 (20) (2011) 1778–1784.
[52] Y. Li, C. Wen, D. Mushahary, R. Sravanthi, N. Harishankar, G. Pande, P. Hodgson, Acta Biomater. 8 (8) (2012) 3177–3188.
[53] D. Mushahary, C. Wen, J.M. Kumar, J. Lin, N. Harishankar, P. Hodgson, G. Pande, Y. Li, Colloids Surf. B Biointerfaces 122 (Oct. 2014) 719–728.
[54] Z. Li, X. Gu, S. Lou, Y. Zheng, Biomaterials 29 (10) (2008) 1329–1344.
[55] S. Zhang, X. Zhang, C. Zhao, J. Li, Y. Song, C. Xie, H. Tao, Y. Zhang, Y. He, Y. Jiang, Y. Bian, Acta Biomater. 6 (2) (2010) 626–640.
[56] Y. Ding, C. Wen, P. Hodgson, Y. Li, J. Mater. Chem. B 2 (14) (2014) 1912–1933.
[57] H.R.B. Rad, M.H. Idris, M.R.A. Kadir, S. Farahany, Mater. Des. 33 (1) (2012) 88–97.
[58] M.B. Kannan, R.K.S. Raman, Biomaterials 29 (15) (2008) 2306–2314.
[59] J. Huang, Y. Ren, Y. Jiang, B. Zhang, K. Yang, Front. Mater. Sci. China 1 (4) (2007) 405–409.
[60] J.M. Seitz, R. Eifler, J. Stahl, M. Kietzmann, F.W. Bach, Acta Biomater. 8 (10) (2012) 3852–3864.

[61] C. Hampp, B. Ullmann, J. Reifenrath, N. Angrisani, D. Dziuba, D. Bormann, J.M. Seitz, A. Meyer-Lindenberg, Adv. Eng. Mater. 14 (3) (2012) 28–37.
[62] C. Hampp, N. Angrisani, J. Reifenrath, D. Bormann, J.M. Seitz, A. Meyer-Lindenberg, Mater. Sci. Eng. C 33 (1) (2013) 317–326.
[63] Y. Li, C. Wen, D. Mushahary, R. Sravanthi, N. Harishankar, G. Pande, P. Hodgson, Acta biomaterialia 8 (8) (2012) 3177–3188.
[64] X.N. Gu, X.H. Xie, N. Li, Y.F. Zheng, L. Qin, Acta biomaterialia 8 (6) (2012) 2360–2374.
[65] N.D. Nam, W.C. Kim, J.G. Kim, K.S. Shin, and H.C. Jung, "Corrosion Resistance of Mg–5Al–xSr Alloys," vol. 509, pp. 4839–4847, 2011.
[66] M. Bornapour, N. Muja, D. Shum-tim, M. Cerruti, M. Pekguleryuz, Acta Biomater. 9 (2) (2013) 5319–5330.
[67] W. An-ru, "Study of the Microstructure and Mechanical Properties of Mg-rare Earth Alloys," vol. 28, pp. 1963–1967, 2007.
[68] H.F. Gao, H.Q. Tan, J. Li, Y.Q. Wang, and J.Q. Xun, "Synergistic Effect of Cerium Conversion Coating and Phytic Acid Conversion Coating on AZ31B Magnesium Alloy," vol. 212, pp. 32–36, 2012.
[69] C. Wen, "Effects of Alloying Elements on the Corrosion Behavior and Biocompatibility of Biodegradable Magnesium Alloys : A Review," no. October, 2014.
[70] K.F. Farraro, K.E. Kim, S.L.-Y. Woo, and B. Jonquil R. Flowers, and Matthew McCullough, "Revolutionizing Orthopaedic Biomaterials: The Potential of Biodegradable and Bioresorbable Magnesium-Based Materials for Functional Tissue Engineering," vol. 100, no. 2, pp. 130–134, 2012.
[71] W. Cheng, S. Ma, Y. Bai, Z. Cui, H. Wang, J. Alloys Compd. 731 (2017) 945–954.
[72] Y. Lu, A.R. Bradshaw, Y.L. Chiu, and I.P. Jones, "Effects of secondary Phase and Grain Size on the Corrosion of Biodegradable Mg–Zn–Ca alloys," vol. 48, pp. 480–486, 2015.
[73] J.J. Ramsden, D.M. Allen, D.J. Stephenson, J.R. Alcock, G.N. Peggs, G. Fuller, G. Goch, CIRP Ann. – Manuf. Technol. 56 (2) (2007) 687–711.
[74] X. Zhang, G. Yuan, J. Niu, P. Fu, W. Ding, J. Mech. Behav. Biomed. Mater. 67 (2012) 74–86.
[75] X. Zhang, G. Yuan, L. Mao, J. Niu, P. Fu, W. Ding, J. Mech. Behav. Biomed. Mater. 7 (2012) 77–86.
[76] C. Zhao, F. Pan, L. Zhang, H. Pan, K. Song, A. Tang, Mater. Sci. Eng. C 70 (2017) 1081–1088.
[77] A. Gil-Santos, I. Marco, N. Moelans, N. Hort, O. Van der Biest, Mater. Sci. Eng. C 71 (2017) 25–34.
[78] Y. Ai, C. Luo, J. Liu, Y. Huang, Jinshu Xuebao/Acta Metall. Sin. 41 (1) (2005) 49–54.
[79] A. Gil-Santos, G. Szakacs, N. Moelans, N. Hort, O. Van der Biest, J. Alloys Compd. 694 (2017) 767–776.
[80] Y. Chen, J. Gao, Y. Song, Y. Wang, Mater. Sci. Eng. A 671 (2016) 127–134.
[81] Y. Zhang, X. Huang, Z. Ma, Y. Li, F. Guo, J. Yang, Y. Ma, Y. Hao, Mater. Sci. Eng. A 686 (2017) 93–101.
[82] S. Bauer, P. Schmuki, K. von der Mark, J. Park, Prog. Mater. Sci. 58 (3) (2013) 261–326.
[83] Y. Shibata, Y. Tanimoto, J. Prosthodont. Res. 59 (1) (2015) 20–33.
[84] D. Deligianni, Biomaterials 22 (11) (2001) 1241–1251.
[85] A.F. van Tol, J.E. Tibballs, N. Roar Gjerdet, P. Ellison, J. Mech. Behav. Biomed. Mater. 28 (2013) 254–262.
[86] T. Scheerlinck, P.-P. Casteleyn, J. Bone Joint Surg. Br. 88–B (11) (2006) 1409–1418.
[87] H.J. Rønold, S.P. Lyngstadaas, J.E. Ellingsen, Biomaterials 24 (25) (2003) 4559–4564.
[88] R.A. Gittens, T. McLachlan, R. Olivares-Navarrete, Y. Cai, S. Berner, R. Tannenbaum, Z. Schwartz, K.H. Sandhage, B.D. Boyan, Biomaterials 32 (13) (2011) 3395–3403.
[89] S.P. Lake, S. Ray, A.M. Zihni, D.M. Thompson, J. Gluckstein, C.R. Deeken, J. Mech. Behav. Biomed. Mater. 42 (2015) 186–197.
[90] L. Prodanov, E. Lamers, M. Domanski, R. Luttge, J.A. Jansen, X.F. Walboomers, Biomaterials 34 (12) (2013) 2920–2927.
[91] N. Sato, K. Kubo, M. Yamada, N. Hori, T. Suzuki, H. Maeda, T. Ogawa, J. Dent. Res. 88 (9) (2009) 812–816.
[92] R. Brånemark, L. Emanuelsson, A. Palmquist, P. Thomsen, Nanomed. Nanotechno. Biol. Med. 7 (2) (2011) 220–227.
[93] N. Mirhosseini, P.L. Crouse, M.J.J. Schmidth, L. Li, D. Garrod, Appl. Surf. Sci. 253 (19) (2007) 7738–7743.
[94] M. Bornapour, M. Celikin, M. Cerruti, M. Pekguleryuz, Mater. Sci. Eng. C 35 (1) (2014) 267–282.
[95] J. Wang, J. Tang, P. Zhang, Y. Li, J. Wang, Y. Lai, L. Qin, J. Biomed. Mater. Res. – Part B Appl. Biomater. 100 B (6) (2012) 1691–1701.
[96] L.N. Zhang, Z.T. Hou, X. Ye, Z. Bin Xu, X.L. Bai, P. Shang, Front. Mater. Sci. 7 (3) (2013) 227–236.
[97] B. Homayun, A. Afshar, J. Alloys Compd. 607 (2014) 1–10.
[98] Y. Yandong, K. Shuzhen, P. Teng, L. Jie, L. Caixia, Metallogr. Microstruct. Anal. 4 (5) (2015) 381–391.
[99] L.B. Tong, Q.X. Zhang, Z.H. Jiang, J.B. Zhang, J. Meng, L.R. Cheng, H.J. Zhang, J. Mech. Behav. Biomed. Mater. 62 (2016) 57–70.
[100] Y. Yan, H. Cao, Y. Kang, K. Yu, T. Xiao, J. Luo, Y. Deng, H. Fang, H. Xiong, Y. Dai, J. Alloys Compd. 693 (2017) 1277–1289.
[101] L. Shi, Y. Huang, L. Yang, F. Feyerabend, C. Mendis, R. Willumeit, K. Ulrich Kainer, N. Hort, J. Mech. Behav. Biomed. Mater. 47 (2015) 38–48.
[102] Z. Zhen, T. Xi, Y. Zheng, L. Li, L. Li, J. Mater. Sci. Technol. 30 (7) (2014) 675–685.
[103] W. Wang, J. Han, X. Yang, M. Li, P. Wan, L. Tan, Y. Zhang, K. Yang, Mater. Sci. Eng. B 214 (2016) 26–36.
[104] X. Zhang, Y. Xue, Z. Wang, Trans. Nonferrous Met. Soc. China 22 (10) (2012) 2343–2350.
[105] Z. Gui, Z. Kang, Y. Li, J. Alloys Compd. 685 (2016) 222–230.
[106] Y. Sun, B. Zhang, Y. Wang, L. Geng, X. Jiao, Mater. Des. 34 (2012) 58–64.
[107] F. Wu, C. Liu, B. O'Neill, J. Wei, N. Yung, Appl. Surf. Sci. 258 (19) (2012) 7589–7595.
[108] S.J. Zhu, Q. Liu, Y.F. Qian, B. Sun, L.G. Wang, J.M. Wu, S.K. Guan, Front. Mater. Sci. 8 (3) (2014) 256–263.
[109] J. Fan, X. Qiu, X. Niu, Z. Tian, W. Sun, X. Liu, Y. Li, W. Li, J. Meng, Mater. Sci. Eng. C 33 (4) (2013) 2345–2352.
[110] Y. Huang, D. Liu, L. Anguilano, C. You, M. Chen, Mater. Sci. Eng. C 54 (2015) 120–132.
[111] S. Zhang, Y. Zheng, L. Zhang, Y. Bi, J. Li, J. Liu, Y. Yu, H. Guo, Y. Li, Mater. Sci. Eng. C 68 (2016) 414–422.
[112] J. Zhang, N. Kong, Y. Shi, J. Niu, L. Mao, H. Li, M. Xiong, G. Yuan, Corros. Sci. 85 (2014) 477–481.
[113] M. Bornapour, M. Celikin, M. Pekguleryuz, Mater. Sci. Eng. C 46 (2015) 16–24.
[114] A. Tahmasebifar, Surface Morphology Investigation of a Biodegradable Magnesium Alloy, Middle East Technical University, 2015.
[115] Y. Zheng, Y. Li, J. Chen, Z. Zou, Corros. Sci. 90 (2015) 445–450.
[116] A.H.M. Sanchez, B.J.C. Luthringer, F. Feyerabend, R. Willumeit, Acta Biomater. 13 (2015) 16–31.
[117] C. Zhao, H. Wu, P. Hou, J. Ni, P. Han, X. Zhang, Mater. Lett. 180 (2016) 42–46.
[118] R. Willumeit, J. Fischer, F. Feyerabend, N. Hort, U. Bismayer, S. Heidrich, B. Mihailova, Acta Biomater. 7 (6) (2011) 2704–2715.
[119] D. Zhao, T. Wang, W. Hoagland, D. Benson, Z. Dong, S. Chen, D.T. Chou, D. Hong, J. Wu, P.N. Kumta, W.R. Heineman, Acta Biomater. 45 (2016) 399–409.
[120] H.R. Bakhsheshi-Rad, M. Abdellahi, E. Hamzah, A.F. Ismail, M. Bahmanpour, J. Alloys Compd. 687 (2016) 630–642.
[121] L. Gao, R.S. Chen, E.H. Han, J. Alloys Compd. 481 (1–2) (2009) 379–384.
[122] F. Li, J. Li, G. Xu, G. Liu, H. Kou, L. Zhou, J. Mech. Behav. Biomed. Mater. 46 (2015) 104–114.
[123] C. Zhao, F. Pan, S. Zhao, H. Pan, K. Song, A. Tang, Mater. Sci. Eng. C 54 (2015) 245–251.
[124] L.J. Liu, M. Schlesinger, Corros. Sci. 51 (8) (2009) 1733–1737.
[125] R. Zeng, J. Zhang, W. Huang, W. Dietzel, K.U. Kainer, C. Blawert, W. Ke, Trans. Nonferrous Met. Soc. China 16 (2006) s763–s771.

[126] B. Zhang, Y. Hou, X. Wang, Y. Wang, L. Geng, Mater. Sci. Eng. C 31 (8) (2011) 1667–1673.
[127] C.A. Grillo, F. Alvarez, M.A.F.L. de Mele, Colloids Surf. B Biointerfaces 117 (2014) 312–321.
[128] H.S. Brar, B.G. Keselowsky, M. Sarntinoranont, M.V. Manuel, Magnes. Technol. 2011 (April) (2011) 401-401.
[129] P.I.K. Kustra, A.N.M. Ilenin, M.I.S. Chaper, and A.L.G. Ridin, "Multi Scale Modeling and Interpretation of Tensile Test of Magnesium Alloys in Microchamber for the Sem," vol. 9, no. 2, pp. 207–214, 2009.
[130] A. Milenin, D.J. Byrska, O. Grydin, Comput. Struct. 89 (11–12) (2011) 1038–1049.
[131] A. Miehe, U. Gross, IOP Conf. Ser. Mater. Sci. Eng. 33 (1) (2012) 12017.
[132] Z. Pu, D. Umbrello, O.W. Dillon, T. Lu, D.A. Puleo, I.S. Jawahir, J. Manuf. Process. 16 (2) (2014) 335–343.
[133] Y.B. Guo, M. Salahshoor, CIRP Ann. – Manuf. Technol. 59 (1) (2010) 151–154.
[134] M. Salahshoor, Y.B. Guo, Int. J. Mach. Tools Manuf. 51 (7–8) (2011) 579–590.
[135] G.G. Lin and J.G. Scott, "Magnesium Alloys as a Biomaterial for Degradable Craniofacial Screws," vol. 100, no. 2, pp. 130–134, 2015.
[136] M. Salahshoor, Y.B. Guo, Int. J. Adv. Manuf. Technol. 64 (1–4) (2013) 133–144.
[137] B. Zberg, P.J. Uggowitzer, J.F. Löffler, Nat. Mater. 8 (11) (2009) 887–891.
[138] R. Willumeit, F. Feyerabend, N. Huber, Acta Biomater. 9 (10) (2013) 8722–8729.
[139] R. Montoya, "Effect of Impurities and Electrolyte Thickness on Degradation of Pure Mg. Study by FEM," pp. 208–231, 2011.
[140] P. Bajger, "Modelling the Corrosion of Magnesium and its Alloys," no. September, pp. 1–6, 2015.
[141] P. Bajger, J.M.A. Ashbourn, V. Manhas, Y. Guyot, K. Lietaert, L. Geris, Biomech. Model. Mechanobiol. 16 (1) (2016) 1–12.
[142] W. Wu, L. Petrini, D. Gastaldi, T. Villa, M. Vedani, E. Lesma, B. Previtali, F. Migliavacca, Ann. Biomed. Eng. 38 (9) (2010) 2829–2840.
[143] W. Wu, D. Gastaldi, K. Yang, L. Tan, L. Petrini, F. Migliavacca, Mater. Sci. Eng. B Solid-State Mater. Adv. Technol. 176 (20) (2011) 1733–1740.
[144] W. Wu, S. Chen, D. Gastaldi, L. Petrini, D. Mantovani, K. Yang, L. Tan, F. Migliavacca, Acta Biomater. 9 (10) (2013) 8730–8739.
[145] D. Gastaldi, V. Sassi, L. Petrini, M. Vedani, S. Trasatti, F. Migliavacca, J. Mech. Behav. Biomed. Mater. 4 (3) (2011) 352–365.
[146] J.A. Grogan, B.J. O'Brien, S.B. Leen, P.E. McHugh, Acta Biomater. 7 (9) (2011) 3523–3533.
[147] N. Debusschere, P. Segers, P. Dubruel, B. Verhegghe, M. De Beule, Ann. Biomed. Eng. 44 (2) (2016) 382–390.
[148] V.H. Carneiro, H. Puga, Modeling and elastic simulation of auxetic magnesium stents, in: Proceedings of the 2015 IEEE 4th Portuguese Meeting on Bioengineering, ENBENG 2015, 2015, pp. 26–28.
[149] E.L. Boland, J.A. Grogan, C. Conway, P.E. McHugh, JOM 68 (4) (2016) 1198–1203.
[150] K. Kusnierczyk, M. Basista, J. Biomater. Appl. 31 (6) (2016) 1–23.
[151] S.C. Cifuentes, E. Frutos, J.L. González-Carrasco, M. Muñoz, M. Multigner, J. Chao, R. Benavente, M. Lieblich, Mater. Lett. 74 (2012) 239–242.
[152] S.C. Cifuentes, M. Lieblich, F.A. López, R. Benavente, J.L. González–Carrasco, Mater. Sci. Eng. C 72 (2017) 18–25.
[153] C.H. Kum, Y. Cho, Y.K. Joung, J. Choi, K. Park, S.H. Seo, Y.S. Park, D.J. Ahn, D.K. Han, J. Mater. Chem. B 1 (21) (2013) 2764.
[154] Y.H. Wu, N. Li, Y. Cheng, Y.F. Zheng, Y. Han, J. Mater. Sci. Technol. 29 (6) (2013) 545–550.
[155] A. Brown, S. Zaky, H. Ray, C. Sfeir, Acta Biomater. 11 (C) (2015) 543–553.
[156] F. Witte, F. Feyerabend, P. Maier, J. Fischer, M. Störmer, C. Blawert, W. Dietzel, N. Hort, Biomaterials 28 (13) (2007) 2163–2174.
[157] B. Chen, K.-Y. Yin, T.-F. Lu, B.-Y. Sun, Q. Dong, J.-X. Zheng, C. Lu, Z.-C. Li, J. Mater. Sci. Technol. 32 (9) (2016) 858–864.
[158] X. Gu, W. Zhou, Y. Zheng, L. Dong, Y. Xi, D. Chai, Mater. Sci. Eng. C 30 (6) (2010) 827–832.
[159] B. Ratna Sunil, T.S. Sampath Kumar, U. Chakkingal, V. Nandakumar, M. Doble, Mater. Sci. Eng. C 39 (1) (2014) 315–324.
[160] A. Feng, Y. Han, Mater. Des. 32 (5) (2011) 2813–2820.
[161] D.B. Liu, M.F. Chen, X.Y. Ye, Front. Mater. Sci. China 4 (2) (2010) 139–144.
[162] X. Ye, M. Chen, M. Yang, J. Wei, D. Liu, J. Mater. Sci. Mater. Med. 21 (4) (2010) 1321–1328.
[163] M. Razavi, M.H. Fathi, M. Meratian, Mater. Lett. 64 (22) (2010) 2487–2490.
[164] M. Razavi, M.H. Fathi, M. Meratian, Mater. Charact. 61 (12) (2010) 1363–1370.
[165] S.Y. He, Y. Sun, M.F. Chen, D.B. Liu, X.Y. Ye, Trans. Nonferrous Met. Soc. China 21 (4) (2011) 814–819.
[166] X. Wang, P. Zhang, L.H. Dong, X.L. Ma, J.T. Li, Y.F. Zheng, Mater. Des. 54 (2014) 995–1001.
[167] K. Yu, L. Chen, J. Zhao, S. Li, Y. Dai, Q. Huang, Z. Yu, Acta Biomater. 8 (7) (2012) 2845–2855.
[168] K. Yu, L. Chen, J. Zhao, R. Wang, Y. Dai, Q. Huang, Mater. Lett. 98 (2013) 22–25.
[169] X.N. Gu, X. Wang, N. Li, L. Li, Y.F. Zheng, X. Miao, J. Biomed. Mater. Res. – Part B Appl. Biomater. 99 B (1) (2011) 127–134.
[170] Z. Huan, J. Zhou, J. Duszczyk, J. Mater. Sci. Mater. Med. 21 (12) (2010) 3163–3169.
[171] Z. Huan, S. Leeflang, J. Zhou, W. Zhai, J. Chang, J. Duszczyk, J. Biomed. Mater. Res. – Part B Appl. Biomater. 100 B (2) (2012) 437–446.
[172] M. Ashuri, F. Moztarzadeh, N. Nezafati, A. Ansari Hamedani, M. Tahriri, Mater. Sci. Eng. C 32 (8) (2012) 2330–2339.
[173] Z. Huan, C. Xu, B. Ma, J. Zhou, J. Chang, RSC Adv. 6 (53) (2016) 47897–47906.
[174] S.N. Dezfuli, Z. Huan, S. Leeflang, J. Chang, J. Zhou, J. Mech. Behav. Biomed. Mater. 67 (2016) 74–86.
[175] S. Xiong, J. Alloys Compd. 702 (January) (2017) 199–208.
[176] M. Radovic and M.W. Barsoum, "MAX Phases: Bridging the Gap Between Metals and Ceramics," vol. 92, no. 3, pp. 20–27.